THE ASTROPHYSICAL JOURNAL, 283:495–511, 1984 August 15

THE MEDIUM SENSITIVITY SURVEY: A NEW SAMPLE OF X-RAY SOURCES WITH OPTICAL IDENTIFICATIONS AND THE REVISED EXTRAGALACTIC LOG N–LOG S[1]

ISABELLA M. GIOIA,[2] TOMMASO MACCACARO,[2] AND RUDY E. SCHILD
Harvard-Smithsonian Center for Astrophysics
JOHN T. STOCKE AND JAMES W. LIEBERT
Steward Observatory, University of Arizona
AND
IVAN J. DANZIGER, DANIEL KUNTH,[3] AND JAN LUB[4]
European Southern Observatory
Received 1983 October 20; accepted 1984 February 29

ABSTRACT

The *Einstein Observatory* Medium Sensitivity Survey has been extended. Forty-nine new, high galactic latitude X-ray sources have been detected in ~150 Imaging Proportional Counter fields (~40 deg^2) with sensitivities in the range 7×10^{-14} to 2×10^{-12} ergs cm^{-2} s^{-1}. The optical program undertaken to identify these new sources has yielded a virtual 100% identification rate. These sources have been combined with those previously selected by Maccacaro *et al.*, giving a resulting sample of 112 serendipitous X-ray sources. Of these, 75% are associated with extragalactic objects, and 25% are identified with galactic stars. Active galactic nuclei (AGNs—quasars and Seyfert galaxies) constitute the large majority of the extragalactic population (68%). They are primarily low-redshift ($z \leq 1$) and low-luminosity objects and, for the most part, are similar to optically or radio-selected quasars. However, about 10% of them have reddish colors ($B-V \geq 0.8$) and would not have been easily discovered by standard color techniques. The increased statistics have allowed a better determination of the number-count relation. A best fit power law of 1.45 ± 0.12 is derived for the extragalactic population as a whole. Furthermore the log N–log S relations for the two classes of objects for which enough statistics are present, AGNs and clusters of galaxies, have been computed. AGNs are described by a fairly steep number-count relation, while the log N–log S of clusters of galaxies is significantly flatter. This result indicates that the sum of different contributions conspire to mimic the "Euclidean" slope of the extragalactic X-ray log N–log S.

Subject headings: galaxies: nuclei — X-ray: sources

I. INTRODUCTION

The two imaging instruments on board the *Einstein Observatory*, the Imaging Proportional Counter (IPC) and the High Resolution Imager (HRI), were not specifically designed to perform a survey of large areas of sky. Nevertheless these instruments have provided a large amount of data used to search for new X-ray sources, to extend the source-count relation of extragalactic objects to fluxes of the order of 10^{-14} ergs cm^{-2} s^{-1}, and to study the nature and type of objects contributing to the diffuse X-ray background.

Giacconi *et al.* (1979) reported on the analysis of several deep exposures (limiting sensitivity $\sim 1.3 \times 10^{-14}$ ergs cm^{-2} s^{-1} in the 1–3 keV energy band) covering ~1 deg^2 of sky in the Draco and Eridanus region. More recently Griffiths *et al.* (1983) extended the "deep survey" to the Pavo region, achieving about the same sensitivity (i.e., 1.1×10^{-14} ergs cm^{-2} s^{-1} in the 1–3 keV band). Unfortunately, only ~20% of the "deep survey" X-ray sources have been identified due to the extreme faintness ($m > 21$) of the large majority of the optical counterparts. Although the deep surveys provide a very faint limit for the source counts, their log N–log S point is highly uncertain due to the large fraction of unidentified sources and to the poor statistics.

Maccacaro *et al.* (1982, hereafter Paper I), surveyed ~50 deg^2 in different regions of the sky at medium sensitivity flux levels (~10^{-13}–10^{-12} ergs cm^{-2} s^{-1} in the 0.3–3.5 keV energy band) intermediate between the *Uhuru*/*Ariel V* limit and the *Einstein* deep survey limit. This "first" medium sensitivity survey (hereafter MSS 1) was primarily aimed at the analysis of the source-count relation for extragalactic X-ray sources. In the flux density range of MSS 1 a best fit power-law slope of 1.53 ± 0.16 for the number-flux relation was found. Since the medium sensitivity survey is carried out by searching for serendipitous sources in IPC fields taken for other purposes, its size can be expanded by adding new fields, and a very large sample of X-ray sources can thus be gathered. This, combined with the capability of satisfactorily identifying virtually all sources with objects visible on the POSS plates, makes an expanded sample the best method for further investigations of the faint X-ray sky, including the possibility of finding unusual or "extreme" objects like the narrow-line reddish AGNs (Stocke *et al.* 1982; Stocke *et al.* 1983, hereafter Paper II). To these ends new IPC fields were analyzed to enlarge the sample of serendipitous X-ray sources. A parallel optical program to identify all the new sources was also undertaken. In this paper X-ray and optical data are presented for this "second" complete sample

[1] Research reported here used the Multiple Mirror Telescope Observatory, a joint facility of the Smithsonian Institution and the University of Arizona.
[2] Also from Istituto di Radioastronomia del CNR, 40126 Bologna, Italy.
[3] Now at Institut d' Astrophysique, F-75014 Paris, France.
[4] Now at the Sterrewacht, 2300 RA Leiden, The Netherlands.

of medium sensitivity survey X-ray sources (MSS 2) selected exactly in the same way as in MSS 1.

In the past 3 years systematic studies of serendipitous *Einstein* sources have been carried out by several authors (e.g., Chanan, Margon and Downes 1981; Kriss and Canizares 1982; Reichert *et al.* 1982; Katgert, Thuan, and Windhorst 1983). The medium survey sample (Paper 1; Paper 2; this paper) has a major advantage with respect to the other samples. It is a large, flux-limited complete catalog of X-ray sources. The 5 σ threshold guarantees that the number of spurious sources is minimized if not nil. Moreover, at any given X-ray flux F_x, the area of sky that has been searched for sources brighter than F_x is known (see Table 1). Thus the medium survey sample is truly representative of the soft X-ray sky at flux levels of $\approx 10^{-13}$ to 10^{-12} ergs cm^{-2} s^{-1} (0.3–3.5 keV). This, combined with the virtual 100% identification rate, allows the determination of the surface density of different classes of sources, their cosmological evolution, and their luminosity function. In what follows only the first of these topics is examined; others will be studied and presented in subsequent papers.

In § II the selection criteria and data analysis are described. The source sample is examined in § III. Section IV presents the optical identification procedure including a discussion of the few sources for which the identification is ambiguous. Section V presents a discussion of the AGNs and BL Lac objects in the sample. The log N–log S relation is derived and discussed in § VI. A brief summary is given in § VII.

II. SELECTION CRITERIA AND DATA ANALYSIS

One hundred forty-nine new IPC fields with limiting sensitivities in the range $\sim 1 \times 10^{-13}$ to $\sim 1 \times 10^{-12}$ ergs cm^{-2} s^{-1} have been analyzed yielding a total area of ~ 40 deg^2 of sky. Forty-nine serendipitous sources have been discovered satisfying the selection criteria used for MSS 1 (Paper I). In the interest of clarity we will briefly summarize these selection criteria. Only the IPC fields outside the galactic plane, $|b^{II}| > 20°$, have been selected to avoid the effects of galactic absorption as well as regions of high stellar density. Fields centered on nearby (distance class ≤ 3) Abell clusters of galaxies were not used in order to avoid including sources physically related to the cluster itself. For each IPC image only the central $32' \times 32'$ has been analyzed both to avoid regions obscured by the window supporting structure and regions in which the positional accuracy is significantly degraded. Moreover, a region of $5'$ radius centered on the target of the observation was discarded. The target objects have been excluded from the sample together with any other source physically related to them. MSS 1 explicitly shows (see Paper I) that this last criterion does not significantly bias the composition of the sample.

Sources are accepted only if the significance of their detection exceeds the (formal) 5 σ level [i.e., source counts/(source counts + background)$^{1/2} \geq 5$] in a $120''$ radius circle centered on the source itself. This high threshold ensures that even in a sample several times larger than the present one, virtually no spurious sources are expected. All the sources found with the above-described procedure were kept, even if they are previously cataloged objects. For some fields a new IPC reprocessing has allowed us to reduce the positional uncertainty from $\sim 1'$ to $30''$, thus reducing the number of possible candidates in the error circle. Unfortunately, due to the demise of the *Einstein Observatory* a few months after the present survey was initiated, only one HRI observation is available (unlike the first sample for which many HRI confirmations existed). Smoothed isocontour X-ray maps were produced for all the sources by convolving the raw data with a $32''$ σ Gaussian function. By inspection of the smoothed maps several sources clearly appeared resolved (see Figure 1). Whenever a second longer IPC observation became available for a field already analyzed as part of MSS 1, the latter was preferred and reanalyzed. Two sources are found to be X-ray variables (see § III and Table 2 for more details) between the two observations.

TABLE 1

THE SKY COVERAGE FOR THE *EINSTEIN* MEDIUM SENSITIVITY SURVEY

Limiting Sensitivity ($\times 10^{-13}$ ergs cm^{-2} s^{-1})	Area (deg^2)
0.7	0.3
1.6	5.8
2.5	24.6
4.5	49.0
6.5	72.3
10.0	87.3
20.0	89.1

NOTE.—Total area = 89.1 deg^2.

III. THE SAMPLE

Combining the 49 sources presented here with the 63 of MSS 1, we have a sample of 112 serendipitous X-ray sources detected in a total area of ~ 90 deg^2 of sky. The sky coverage as a function of the limiting X-ray flux is given in Table 1. Each field yields an area of ~ 0.27 deg^2. The exposure times of the observations range from $\sim 10^3$ to $\sim 2.5 \times 10^4$ s. Most of the objects lying inside or immediately outside the 90% confidence error circle were spectroscopically examined. The identification process and its reliability are described in § IV. VLA observations at 6 cm were performed for all the X-ray sources lying north of declination $\delta = -20°$ which were considered to be associated with extragalactic objects on the basis of the X-ray to visual flux ratio, f_x/f_v, of the optical candidates in the error circle [$\log f_x/f_v = \log f_x + (m_v/2.5) + 5.37$], where f_x is the X-ray flux in ergs cm^{-2} s^{-1} in the 0.3–3.5 keV band and m_v is the visual apparent magnitude. For each source detected at 6 cm (approximately one-third of the extragalactic sample), the radio position is consistent with the position of the object independently proposed as the optical counterpart of the X-ray source. The VLA observations are thus an efficient complement to optical work in validating the proposed identifications (for details, see Feigelson, Maccacaro, and Zamorani 1982, and Gioia *et al.* 1983). In Table 2 all the relevant parameters for the 49 new X-ray sources are given together with their proposed identification. Columns are as follows:

Col. (1). The *Einstein* source name using the same notation as in Paper I. A plus sign (+) indicates sources for which notes appear at the end of the table.

Col. (2). The position of the X-ray centroid in 1950.0 coordinates (right ascension and declination).

Col. (3). The radius of the 90% confidence X-ray error circle being $30''$ or $60''$ according to the availability of the improved IPC positions. Only one source was observed and redetected with the HRI yielding a $4''$ positional accuracy.

Col. (4). The significance of the detection in number of sigmas.

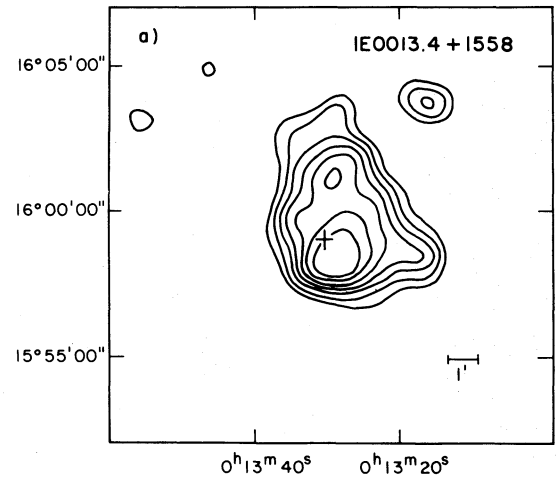

FIG. 1a

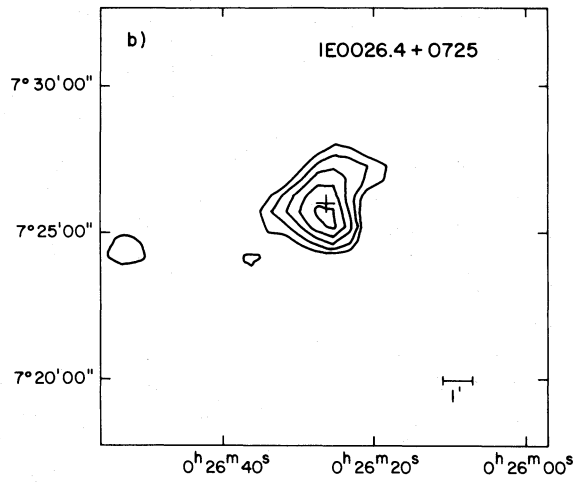

FIG. 1b

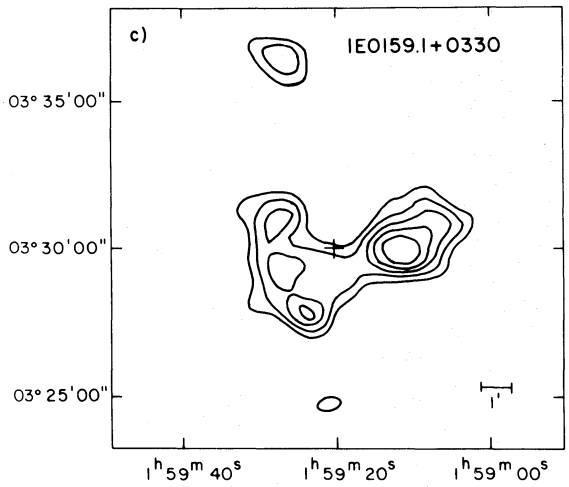

FIG. 1c

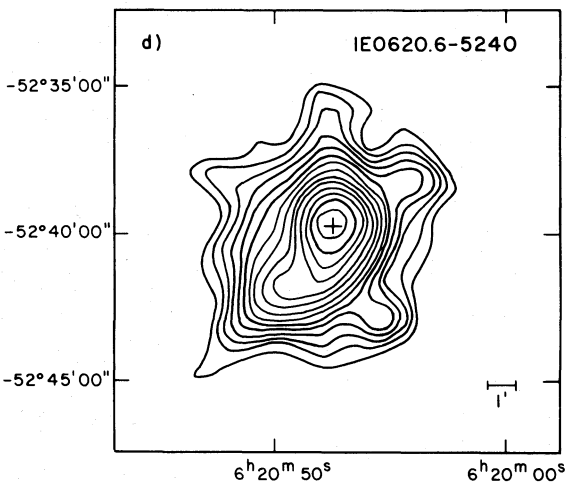

FIG. 1d

FIG. 1.—Isointensity X-ray contours obtained by smoothing the image data with a 32″ Gaussian for the following sources: (*a*) 1E 0013.4+1558. The first contour is 3 σ above the background; the other contours follow in steps of 1 σ. (*b*) 1E 0026.4+0725. Same contour confidence levels as in Fig. 1*a*. (*c*) 1E 0159.1+0330. See notes to Table 2 for this source. Same contours as in Figs. 1*a* and 1*b*. (*d*) 1E 0620.6−5240. Contour levels correspond to 3 σ, 4 σ, 5 σ, 6 σ, 7 σ, 8 σ, 9.5 σ, 10.5 σ, 11.5 σ, 13 σ, 14.5 σ, 16 σ, 18 σ, and 20 σ over background. The plus sign marks the center of the finding charts in Fig. 2.

Col. (5). The X-ray flux of the source computed in the 0.3–3.5 keV band and the 1 σ error (from photon counting statistics only) in units of ($\times 10^{-13}$) ergs cm^{-2} s^{-1}. The flux was estimated assuming a power-law spectrum with an energy slope of 0.4 and corrected for absorption through our own Galaxy assuming an average value of 3.0×10^{20} atoms cm^{-2} for the column density of hydrogen.

Col. (6). The proposed optical identification, always indicated by the letter A in the finding charts. The following abbreviations are used: AGN = active galactic nucleus; Cl = group or cluster of galaxies; BL Lac = BL Lacertae type object; G = "normal" galaxy; Star = star; spectral type is given in the Appendix. In a few cases there is some ambiguity to the identifications. These are listed in Table 3 and discussed in Section IV.

Col. (7). Redshifts uncorrected for galactic or terrestrial motion. When the source identification is a cluster of galaxies, the redshift is the mean for those galaxies observed (see the Appendix). When more than one galaxy was observed, the quoted error is the velocity dispersion.

Col. (8). Visual magnitudes of the proposed identifications: two digits after the decimal point indicate photometric data (see § V); one digit after the decimal point means that the magnitude was estimated from the POSS E prints using the system of King and Raff (1977) and crudely verified by the spectrophotometry obtained in the identification process. Magnitudes for SAO stars are taken from the *SAO Catalog*.

Col. (9). General comments, including X-ray and spectroscopic remarks as well as radio data from the VLA survey of this sample by Gioia *et al.* (1983). References are also given to previous optical work on the proposed identification.

As mentioned above, a plus sign (+) indicates sources for which notes appear at the end of Table 2. Two sources, 1E 0622.5−5256 and 1E 1205.8+6427, are found to be variable in X-rays. 1E 0622.5−5256 had been detected in MSS 1 (Paper I) at a flux of $(6.78 \pm 1.34) \times 10^{-13}$ ergs cm^{-2} s^{-1}. In a second exposure taken 10 months later, its flux had decreased by a factor of $\sim$2.5 to $(2.82 \pm 0.4) \times 10^{-13}$ ergs cm^{-2} s^{-1}. Since this source is almost completely obscured by Canopus opti-

TABLE 2

THE X-RAY SOURCE SAMPLE AND ITS OPTICAL IDENTIFICATION

Source Name	R.A. Dec.	Error Circle	Sigma	Flux(E-13) Error(E-13)	Id	z	m v	Comments
1E0013.4+1558 +	0 13 27.9 15 58 23.7	60"	10.0	7.01 .69	Cl	.083 ±.005	14.7	X-ray extended (see Fig.1 and Table 3)
1E0015.1+1603	0 15 10.2 16 3 34.6	60"	5.5	1.93 .35	Star		7.4	F5,SAO 091825
1E0026.4+0725	0 26 26.4 7 25 59.0	60"	5.5	6.07 1.11	Cl	.170 ±.001	18.27	S(6cm)=2.7 mJy (see Fig.1)
1E0037.7-0157	0 37 44.9 -1 57 27.2	60"	5.9	2.25 .38	AGN	.296 ±.003	17.73	
1E0038.0+3242 +	0 38 1.1 32 42 01.8	30"	6.2	2.20 .35	AGN	.197 ±.003	18.06	(see Table 3)
1E0038.7+3251	0 38 44.9 32 51 22.3	30"	9.0	3.38 .38	AGN	.225 ±.003	18.52	
1E0038.8-0159 +	0 38 51.9 -1 59 53.7	60"	8.4	3.55 .42	AGN	1.690 ±.003	16.86	4C-02.04 S(6cm)=322 mJy
1E0104.2+3153 +	1 4 13.9 31 53 31.7	30"	6.1	4.01 .66	AGN/Cl	2.027 ±.001	18.72	(see Table 3)
1E0116.3-0116	1 16 19.2 -1 16 9.7	60"	9.4	9.65 .88	G	.045 ±.001	15.59	S(6cm)=1.1 mJy
1E0159.1+0330 +	1 59 9.5 3 30 12.3	60"	5.0	3.85 .77	Cl	.165 ±.005	17.5	Abell 293 (see Fig.1 and Table 3)
1E0233.7+0649	2 33 44.5 6 49 11.7	60"	5.5	2.31 .42	Star		13.7	K5(e), weak Hα emission
1E0302.5+1716 +	3 2 30.9 17 16 40.1	30"	5.4	1.88 .34	Cl	.38 ±.04	20.20	
1E0302.7+1658 +	3 2 44.6 16 58 28.0	30"	8.6	3.16 .37	Cl	.39 ±.04	20.13	S(6cm)=3.3 mJy
1E0303.8+1717	3 3 53.3 17 17 00.6	30"	6.6	2.06 .31	Star		8.7	early K, SAO 093280
1E0317.0+1835	3 17 1.4 18 35 24.4	60"	19.5	88.5 4.50	BL Lac	.190 ±.003	18.12	S(6cm)=17 mJy
1E0317.7-6646	3 17 45.3 -66 46 57.7	30"	13.9	1.17 .85	Star		17.1:	M star
1E0326.6-2009	3 26 39.8 -20 9 3.9	60"	5.6	4.88 .87	Star		8.9	F8,SAO 168572 (see Table 3)
1E0331.1-0522	3 31 6.5 -5 22 1.5	30"	6.7	3.29 .49	AGN	.139 ±.001	17.26	
1E0334.2+0025 +	3 34 13.3 0 25 18.1	60"	134	1150 8.60	Star		6.1	G0,SAO 111291 HR 1099, RSCVn
1E0457.9-0555	4 57 57.9 -5 55 57.7	60"	5.4	3.89 .72	AGN	.303 ±.001	17.94	
1E0620.6-5240 +	6 20 36.8 -52 40 14.8	30"	19.3	16.8 .87	Cl	.048 ±.002	15.1:	PKS 0620-52
1E0622.5-5256 +	6 22 33.7 -52 56 11.4	30"	7.0	2.82 .40	Class 1			X-ray variable
1E0623.6-5238 +	6 23 38.6 -52 38 46.5	30"	7.2	2.61 .36	Cl	.074 ±.003	18.0:	obscured by Canopus
1E0730.3+6547	7 30 19.7 65 47 00.7	4"	9.5	6.30 .66	Star		8.5	G0,SAO 014241
1E0920.5+7838	9 20 34.8 78 38 45.3	60"	7.1	5.87 .82	Star		6.5	G0,SAO 006845 (see Table 3)

TABLE 2—*Continued*

Source Name	R.A. Dec.	Error Circle	Sigma	Flux(E-13) Error(E-13)	Id	z	m v	Comments
1E1018.1+2010	10 18 9.8 20 10 34.3	60"	12.1	5.45 .45	AGN	.250 ±.001	18.54	
1E1112.6+4059	11 12 36.2 40 59 48.4	60"	16.2	20.1 1.24	AGN	.076 ±.001	17.10	
1E1137.5+6555	11 37 29.1 65 55 23.5	30"	5.0	1.83 .36	AGN	.397 ±.001	19.48	
1E1205.8+6427	12 5 49.0 64 27 13.0	60"	10.0	6.74 .67	AGN	.105 ±.001	17.70	X-ray variable
1E1216.1+2819	12 16 8.9 28 19 33.2	60"	5.1	1.74 .34	Star		15.2	dMe
1E1218.1+7538	12 18 11.4 75 38 33.0	60"	13.5	6.37 .47	G	.0058 ±.0001	13.12	NGC 4291
1E1218.7+7522	12 18 44.9 75 22 18.1	60"	8.6	3.47 .41	AGN	.645 ±.001	18.16	
1E1220.0+7542	12 20 .6 75 42 19.8	60"	8.3	3.09 .37	Cl	.240 ±.002	18.7	S(6cm)=1.9 mJy
1E1235.4+6315	12 35 28.5 63 15 55.3	60"	12.7	17.8 1.40	BL Lac	.297 ±.002	18.52	S(6cm)=15.2 mJy
1E1253.6-0539	12 53 38.2 -5 39 49.4	60"	5.9	1.31 .22	AGN	.420 ±.002	19.97	
1E1430.4+0527	14 30 27.4 5 27 12.6	60"	8.2	6.63 .81	AGN	.202 ±.003	17.92	
1E1439.8-0520	14 39 53.1 -5 20 42.1	60"	5.0	2.53 .50	AGN	.620 ±.003	17.24	
1E1522.1+3003 +	15 22 8.2 30 3 26.7	60"	22.2	65.1 2.93	Cl	.116 ±.002	16.0:	A2069 (Gioia et al. 1982)
1E1553.6+1558	15 53 36.2 15 58 9.6	60"	7.4	7.18 .96	AGN	1.324 ±.001	17.68	
1E1604.8+1552	16 4 53.6 15 52 7.3	60"	7.4	4.02 .54	AGN	.357 ±.001	19.07	
1E1611.8-0324	16 11 50.6 -3 24 7.0	30"	5.3	3.48 .66	AGN	.298 ±.002	17.62	
1E1614.8+0533	16 14 52.4 5 33 36.8	60"	6.3	1.73 .27	AGN	.855 ±.003	18.47	S(6cm)=16 mJy
1E2124.8-1459 +	21 24 49.9 -14 59 39.3	30"	6.1	2.53 .42	AGN	.057 ±.001	14.68	
1E2125.9-1456	21 25 54.3 -14 56 40.2	30"	7.8	2.71 .35	AGN	.304 ±.001	18.13	
1E2134.0+0017 +	21 34 1.5 0 17 52.2	30"	6.3	2.21 .35	Star		15.5	
1E2159.5-5714	21 59 30.1 -57 14 22.3	60"	9.0	11.0 1.20	AGN	.083 ±.003	15.5:	
1E2316.3-4222	23 16 23.2 -42 22 58.0	30"	28.0	27.8 .99	Cl	.054 ±.001	14.5:	PKS 2316-423
1E2318.2-4219	23 18 15.5 -42 19 59.0	30"	7.5	3.15 .42	AGN	.212 ±.002	17.0:	
1E2348.6+1956	23 48 40.8 19 56 55.5	30"	8.9	5.56 .62	AGN	.043 ±.001	17.12	S(6cm)=2.2 mJy
1E2349.9+1951 +	23 49 57.1 19 51 10.5	30"	5.5	3.32 .60	Star		11.0	(see Table 3)

NOTES TO TABLE 2

1E 0013.4+1558.—Although the proposed counterpart is a cluster of galaxies, two stars (objects A and E in finding charts of Fig. 2 and in the Appendix) could be responsible for part of the X-ray emission. This source has been included in the samples used to determine both the extragalactic and cluster source-counts.

1E 0038.0+3242.—This source has been included in the samples used to determine both the extragalactic and AGN source counts.

1E 0038.8−0159.—Redshift for this QSO comes from Strittmatter *et al.* (1974). We confirm this redshift with a short observation at the Steward 2.3 m telescope which detected Si IV, C IV, He II λ1640 and C III] in the 3400–6400 Å region.

1E 0104.2+3153.—Both the galaxy and the quasar are consistent with being the X-ray emitter. See also Table 3. This source has been included in the sample used to determine both the extragalactic and AGN source counts.

1E 0159.1+0330.—Isocontour map for this source, identified with the cluster of galaxies A293 ($D = 6$, $R = 2$), is presented in Fig. 1*c*. The flux given refers only to the west peak which is consistent with the galaxy indicated by an A in the finding chart of Fig. 2. This source has been included in the samples used to determine both the extragalactic and cluster source counts. The two galaxies indicated as C and D account for the northeast source at 015927.2 +033006.6, which was detected at 4.5 σ and, therefore, is not listed in Table 2. The flux of this northeast source is $(3.23 \pm 0.73) \times 10^{-13}$ ergs cm^{-2} s^{-1}. Both galaxies have the same redshift as galaxy A. The southeast peak, a 4.6 σ detection at 015925.0+032803.6 and $F_x = (3.5 \pm 0.75) \times 10^{-13}$ ergs cm^{-2} s^{-1}, is positionally coincident with a quasar ($z \approx 1.90$), which is unrelated to the cluster and probably responsible for this southeast source. Also present in this field is a strong point radio source PKS 0159+034 (Gioia *et al.* 1983) whose position is not coincident with any of the X-ray or optical sources discussed here.

1E 0302.5+1716.—A distant cluster of galaxies is visible on a CCD frame of this field. The redshifts of the brightest four galaxies have been determined from *B*, *V*, *R* photometry.

1E 0302.7+1658.—The brightest member of a distant rich cluster visible on a CCD frame is the VLA radio source. The redshift of this galaxy has been determined from *B*, *V*, *R* photometry.

1E 0334.2+0025.—This source is identified with the well known RS CVn system HR 1099 (e.g., Fraquelli 1982). HR 1099 was the target of several *Einstein* observations. We have detected it as a serendipitous source in an IPC field centered on 10 Tau.

1E 0620.6−5240.—This field is partially obscured by Canopus. The X-ray emission is very extended (see Fig. 1). A G5 star of 7.5 mag (see Table 3 and Appendix) could be responsible for the X-ray emission associated with the northeast clump. This source has been included in the samples used to determine both the extragalactic and cluster source counts.

1E 0622.5−5256.—This source was already detected in MSS 1 and it is now found to be variable in X-rays. It has no firm optical identification as yet although object E is a possible BL Lac object. The f_x/f_v ratios of the candidate objects present in the error circle (see Table 5) support the probable identification with an extragalactic object. It has been included in the sample used to determine the extragalactic log N–log S.

1E 0623.6−5238.—This field is so obscured by Canopus that no finding chart is available from the ESO or SCR Schmidt plates. See the last plate of Fig. 2 for a finding chart of this source. The identification is not yet certain, but it is possibly a cluster of galaxies. This source has been included in the samples used to determine both the extragalactic and cluster log N–log S.

1E 1522.1+3003.—The finding chart for this field has already been published in Gioia *et al.* (1982); the X-ray flux of A2069 reported there was computed in the 0.4–3.0 keV band. This accounts for the difference with respect to the flux presented here which is computed in the 0.3–3.5 keV band.

1E 2124.8−1459.—The galaxy is a weak Seyfert (see Fig. 4). If the $m_v = 14.4$ G star were the X-ray emitter, its log $(f_x/f_v) = -1.5$ would be an order of magnitude higher than others in its spectral class (see Paper II).

1E 2134.0+0017.—We have identified this source with a 15.5 mag K star even though its log $(f_x/f_v) = -1.1$ is an order of magnitude higher than X-ray stars of similar spectral type. However, no other plausible candidate lies within the error circle. The extremely high f_x/f_v ratio could be explained if this source is a RS CVn system. At present we do not have any evidence to support this hypothesis.

1E2349.9+1951.—This source was excluded from the sample used to determine the extragalactic source counts.

cally, it has no firm optical identification as yet, although the object denoted E in this field (see Appendix and finding chart) is a possible BL Lac object. The source 1E 1205.8+6427 was not detected in MSS 1 (3 σ upper limit of 4.8×10^{-13} ergs cm^{-2} s^{-1}). In a subsequent observation taken 12 months later, the source was detected at a flux level of $(6.74 \pm 0.67) \times 10^{-13}$ ergs cm^{-2} s^{-1} and is now identified with an AGN.

Finding charts for all fields are given in Figure 2 (Plates 10–13). The center of each finding chart is coincident with the X-ray position listed in the second column of Table 2. The scale is shown in the first chart. For those sources with resolved X-ray structures, the center of the finding charts is marked with a plus sign in Figure 1. Letters designate objects actually observed spectroscopically. A description of the optical properties for all lettered objects is given in the Appendix.

The IPC field centered on Canopus contains three sources in the medium survey. The presence of Canopus in the field so obscures the ESO and SRC Schmidt photographs that the finding charts we have thus far presented for these sources have been of poor quality. However, we obtained, courtesy of Dr. C. Jones, a red 90 minute plate (emulsion IIIa-F) of the Canopus region taken through a RG 630 filter on the UK Schmidt telescope on the night of 1978 November 28/29. The three new, much-improved finding charts made from this plate are also shown in the last plate of Figure 2.

IV. THE IDENTIFICATION PROCESS AND ITS RELIABILITY

The optical identifications of the survey have the following percentage breakdown: stars constitute 25%, AGNs are 51%, clusters or groups of galaxies are 16%, and the remaining 7% are BL Lac objects and "normal" galaxies. The "normal" galaxies are distinguished from AGNs in that they contain no emission lines in their optical spectra. A detailed discussion of the X-ray and optical properties of one of these galaxies (NGC 4156 ≡ 1E 1208.2+3945 in Paper I) has been presented by Elvis *et al.* (1981). One source (~1%) is still unidentified, and three sources have possible identifications ambiguous between the classes of optical objects listed above. In the computation of these percentages, the sources with ambiguous identification have been assigned to the various classes according to the classification in Table 2 and Notes to Table 2. Based upon the f_x/f_v ratios of the candidate objects present in the error circle, the still unidentified source is of probable extragalactic origin.

The procedure used to identify the optical counterparts of MSS 2 sources is very similar to that employed in MSS 1 (in particular see Paper II for details of the optical observing procedure). The experience gained in identifying the sources of MSS 1 has helped us to be more selective in our optical observing. When an optical object was found whose f_x/f_v ratio was appropriate for its class, we did not always continue to observe objects as we had done before, unless there were other obvious candidates (e.g., other faint BSOs, galaxies, or radio sources). The f_x/f_v values computed were interpreted in terms of the m_v vs. log (f_x/f_v) plot (Fig. 3 in Paper II) with further refinement for the bright stars according to their spectral class (Fig. 4 in Paper II). VLA radio positions validated many identifications made prior to the radio observing and in a few cases provided candidate identifications later verified by spectroscopy.

Without the use of the HRI to verify the optical identifications, a few sources in MSS 2 have ambiguous identifications (see Table 3). Two sources, 1E 0326.6−2009 and 1E 0920.5 +7838, involve close associations of bright stars; one, 1E

TABLE 3

X-RAY SOURCES WHOSE IDENTIFICATIONS ARE AMBIGUOUS

Source	Object Classification	m_v	log (f_x/f_v)	Comments
A. Sources with Two or More Stellar Identifications				
1E 0326.6−2009.....	*A late F	8.90	−3.4	
	B mid G	12.50	−1.9	Marginally high in f_x/f_v for their spectral class.
	C early G	12.50	−1.9	
1E 0920.5+7838.....	*A G star	6.50	−4.6	
	B late F star	6.50	−4.6	
B. Sources with One Galactic and One Extragalactic Identification				
1E 0038.0+3242.....	*A galaxy	18.06	−0.1	$z = 0.197$; absorption spectrum with possible weak Hβ, Hγ, and [O III] emission. Hα falls in A band.
	B early K star	13.80	−1.8	Marginally too high in f_x/f_v.
1E 2349.9+1951.....	*A early K	11.00	−2.7	At the edge of the 90% error circle.
	B late G/early K	14.50	−1.3	Half a decade too high in f_x/f_v.
	C galaxy	16.98	−0.3	$z = 0.084$; absorption spectrum only.
C. Sources with Two Extragalactic Identifications				
1E 0104.2+3153.....	*A galaxy	16.02	−0.6	Giant elliptical at center of compact group; $z = 0.11$.
	*C quasar	18.88	0.5	Broad absorption-line QSO at $z = 2.03$; see Stocke *et al.* 1984 for detailed discussion.
D. Sources of Probable Composite Nature (the values of f_x/f_v for the following sources use estimated f_x from a very uncertain deconvolution of each source				
1E 0013.4+1558.....	*A early G star	11.80	−2.5	See Notes to Table 2.
	*B, C, D galaxies	14.7–14.0	−0.4	$z = 0.079$–0.086.
	*E mid M(e)	16.0	−1.1	Hydrogen emission, See Notes to Table 2.
1E 0159.1+0330	*A–D galaxies	17.5–19.0	−0.2	$z = 0.160$–0.170, A293.
	*F AGN	20.5	+1.1	$z = 1.897$, responsible for SE X-ray source only. See Notes to Table 2.
1E 0620.6−5240.....	*A–E galaxies	15.1–17.0	−0.5	$z = 0.044$–0.050.
	*F G5 star	7.5	−4.0	See Notes to Table 2.

NOTE.—Asterisks indicate the proposed identification.

0104.2+3153, involves the close projection (10″) of a giant elliptical galaxy ($z = 0.11$) at the center of a compact group of galaxies with a broad absorption-line QSO ($z = 2.03$). This unusual projection and its unique attributes (Ca II H and K absorption at $z = 0.11$ in the QSO spectrum, possible gravitational lensing by halo stars of the giant elliptical) have been discussed in detail by Stocke *et al.* (1984).

Two other sources in Table 3 are of concern because of the confusion between a galaxy and a bright galactic star. In MSS 1 we noted the presence of several reddish quasars with prominent narrow emission lines (both permitted and forbidden) and large Hα/Hβ ratios. In MSS 2 we have identified two moderate redshift galaxies (1E 0038.7+3251, $z = 0.225$, and 1E 2124.8−1459, $z = 0.057$) as AGNs due to the presence of broad Hα emission despite the absence or weakness of emission lines further to the blue (see Fig. 4). Because of this it seems possible that some AGNs would be difficult to identify as such, especially when Hα is redshifted beyond the usual observing range. The chance presence of an absorption line galaxy in the two X-ray error circles in Table 3B is very unlikely (~1 in 10^5) strongly suggesting that one or both of these galaxies are X-ray emitters. Here we discuss these two sources in turn to justify our proposed identification in each case:

1E 0038.0+3242.—Both a galaxy ($m_v = 18.06$, $z = 0.197$) and a bright early K star ($m_v = 13.8$) are within the revised 30″ error circle. If the early K star is the X-ray emitter, its log (f_x/f_v) is −1.8, which is a bit high for its spectral class [although three detected G and K stars in MSS 1 have log (f_x/f_v) > −1.8]. The galaxy has weak Hβ, Hγ, and [O III] in emission. Hα was not clearly detected, although it falls at the edge of the atmospheric A band, so its presence cannot be

excluded. Based upon the high f_x/f_v ratio of the star we favour the galaxy as the X-ray emitter.

1E 2349.9+1951.—An 11th mag early K star is at the edge of the X-ray error circle. Closest to the X-ray centroid is a 14.5 mag late G/early K star, and also within the circle is a 16.98 mag galaxy ($z = 0.084$). Their log (f_x/f_v) values are -2.7, -1.3, and -0.3, respectively. The galaxy has elliptical morphology on the POSS and no obvious emission lines in its spectrum, although very weak Hα emission may be present. Based upon the consistent log (f_x/f_v) value, we assign the X-ray emission to the K star.

Based upon the MSS 1 identifications, we noted in Paper II that it was possible to separate galactic from extragalactic sources at a very high confidence level, using data from the POSS alone (see Fig. 3 in Paper II). In MSS 1 one galactic X-ray source, a cataclysmic variable, is indistinguishable from QSOs in the sample prior to optical spectroscopy. One other source in MSS 1 (1E 0809.8+4809) and now the two additional sources in MSS 2 discussed above, have galactic/extragalactic ambiguity despite improved IPC positions. Thus combining MSS 1 and MSS 2, the success rate for distinguishing galactic from extragalactic X-ray sources prior to optical spectroscopy is approximately 96%. It is encouraging that, especially with 30″ positional accuracy, statistical studies of X-ray sources (e.g., the log N–log S diagram for extragalactic sources) can be carried out for large samples without incurring the enormous amount of optical telescope time necessary to spectroscopically identify all the sources.

V. THE ACTIVE GALACTIC NUCLEI AND BL LACERTAE OBJECTS

That X-ray surveys preferentially select low-luminosity AGNs has been noted and discussed in several previous investigations (see Maccacaro and Gioia 1983 and references therein) and even has a suggested physical interpretation based upon accretion disk models of the emission mechanism responsible for the optical light and X-rays (Tucker 1983). The redshift, optical luminosity, and α_{ox} [$\alpha_{ox} = -\log(L_x/L_o)/2.605$] distributions for the medium survey (MSS 1 + MSS 2) sample of AGNs are shown in Gioia and Maccacaro (1983) and are similar to those of previously published X-ray selected samples (e.g., Margon, Chanan, and Downes 1982; Kriss and Canizares 1982; Reichert *et al.* 1982), particularly in that they confirm the preference for low optical luminosity objects. A detailed discussion of the link between optically and X-ray selected AGNs is the subject of a future paper. Also in a related paper in this issue (Maccacaro, Gioia, and Stocke 1984) we present a study of the X-ray luminosity function and its evolution, including an estimate of the AGN contribution to the X-ray background.

Herein we briefly comment on the unusual optical properties (spectra and colors) of a few (~10%) of the AGNs and BL Lac objects in our sample.

Figure 3 shows the spectra of three AGNs which are representative of the medium survey sample. Approximately 90% of the AGNs discovered thus far in the medium survey have an optical spectrum like those in Figure 3 and thus are very

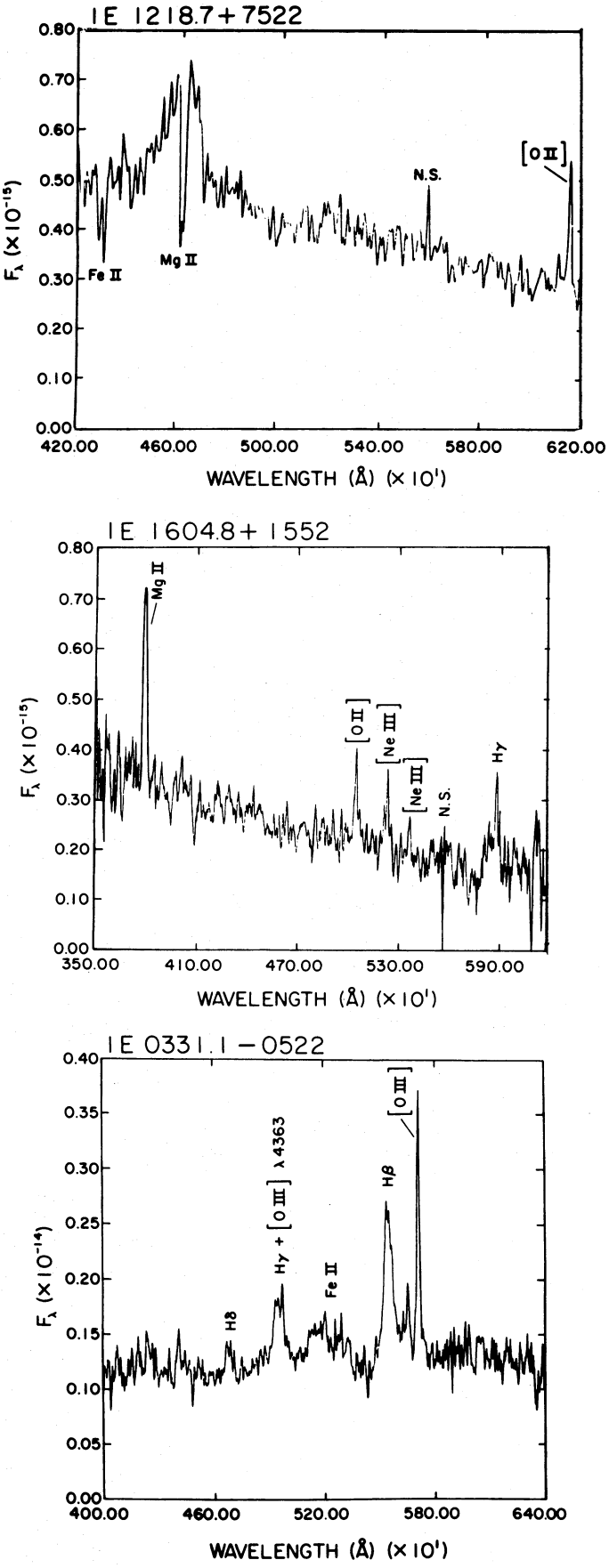

FIG. 3.—Spectra of the three X-ray selected AGNs: 1E 1218.7+7522, 1E 1604.8+1552, and 1E 0331.1−0522. The first two of these are typical of the majority of X-ray selected AGNs in that they possess strong blue continua and permitted lines broader than forbidden lines (type 1 spectra). 1E 0331.1−0522 has a more neutral to reddish continuum ($B-V = 0.76$). In the spectrum of 1E 1218.7+7522 a very strong absorption system is seen in Mg II and Fe II at the emission-line redshift of the [O II] forbidden line to within the errors ($z_{abs} = 0.642 \pm 0.002$; $z_{em} = 0.645 \pm 0.002$).

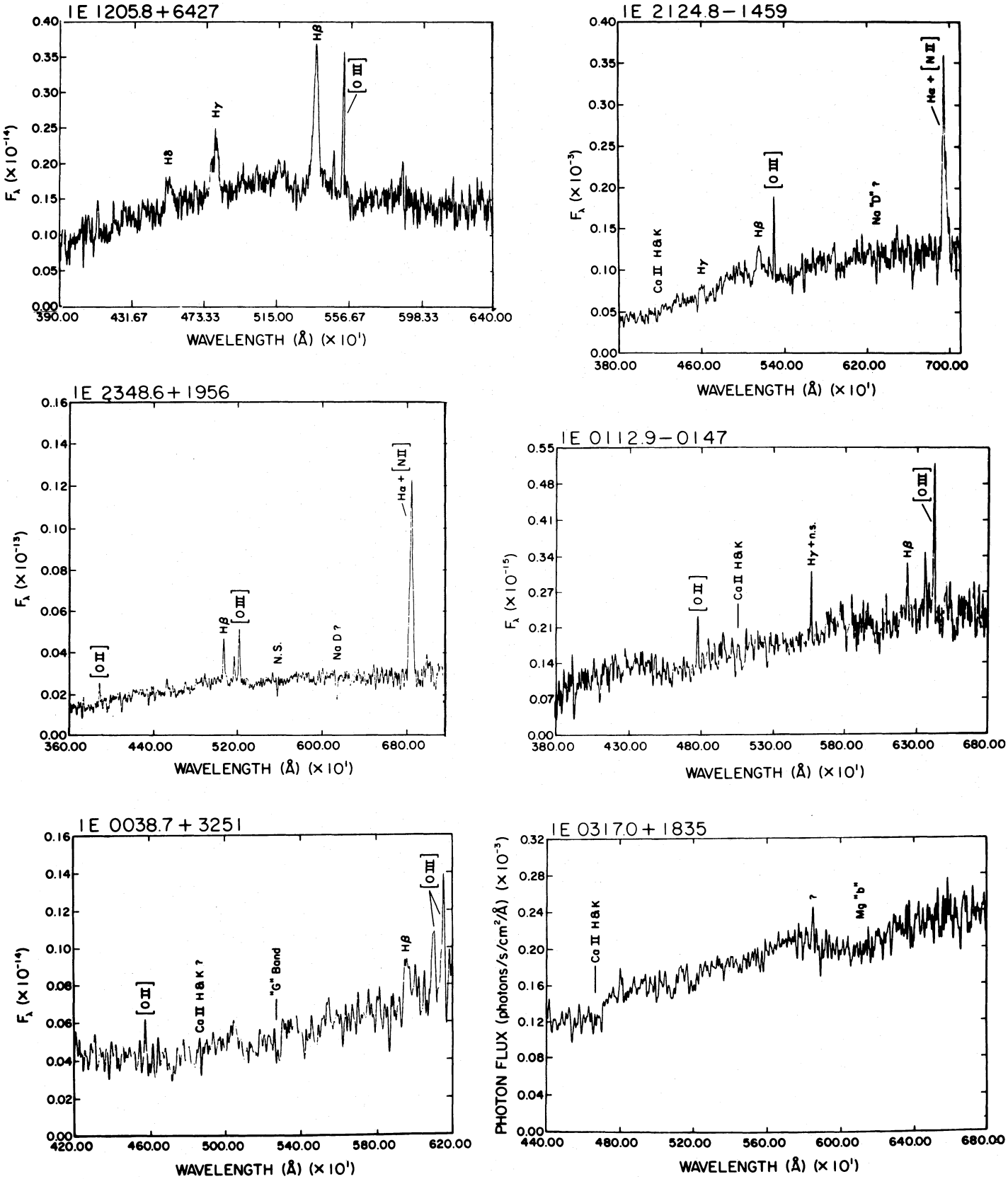

FIG. 4.—A composite figure illustrating the varying types of spectra found among the reddish X-ray selected AGNs and BL Lac objects. 1E 1205.8+6427, despite its $B-V = 0.81$, has a typical type 1 spectrum and no evidence of stellar absorption. 1E 2124.8−1459 contains obvious stellar absorption and permitted emission lines somewhat broader than the forbidden lines. This AGN is clearly extended on the POSS. 1E 2348.6+1956 has a type 2 spectrum, possible Na D absorption, and some weak evidence for a possible H and K break and G band. This AGN is also extended on the POSS. 1E 0112.9−0147 (MSS 1 object; see Paper II) and 1E 0038.7+3251 are higher redshift and fainter versions of the last two spectra above. Each shows some evidence for stellar absorption and rather weak emission lines. 1E 0317.0+1835, an X-ray selected BL Lac object, contains weak absorption features in the spectrum at $z = 0.19$.

similar to optically or radio selected quasars and Seyfert galaxies. Many of the remaining 10%, however, are so unusual in their optical properties as to sometimes cast doubt on their classification. See in particular the optical spectra of 1E 0112.9 −0147 (MSS 1) and 1E 0038.7+3251 (in Fig. 4 herein) which show only weak emission lines not unlike many "normal" spiral galaxies. Likewise, the presence of weak but rather obvious stellar absorption features in the BL Lac candidate 1E 0317.0+1835 (also shown in Fig. 4) is not typical of radio-selected BL Lac objects (see several papers in Wolfe 1978).

We have previously noted (Paper II) the presence in MSS 1 of a few AGNs with unusual "reddish" colors ($B-V \gtrsim 0.8$), similar to normal galaxies. We can now verify this result by means of MSS 2 and with the help of three-color photometry (B, V, R) obtained with the CfA CCD camera.

All AGNs in MSS 1 and MSS 2 with declination north of −20° were observed during the period 1982 May 17–1983 February 12 with the 61 cm telescope of the Whipple Observatory. The filters and detector were as in Schild (1984). The standard exposure times were 10 minutes with each filter, but for approximately 5% of the sources the exposure was doubled because of the faintness of the target object. Twelve stars in M67, covering a range of 1.5 mag in ($B-V$), were repeatedly observed each night for the determination of the extinction and magnitude zero point. A detailed analysis of the data is still in progress; at present we consider our magnitudes and colors to be uncertain by 0.05 mag.

The photometry reported in Table 4 was derived using a 7.″2 diameter (10 pixels) aperture.

Table 4 is organized as follows:

Col. (1). Source name.

Col. (2). Redshift.

Col. (3). V magnitude.

Col. (4). ($B-V$) color.

Col. (5). ($V-R$) color in the Johnson (1966) system.

Col. (6). Galactic longitude l^{II}.

Col. (7). Galactic latitude b^{II}.

Col. (8). ($B-V$) color excess due to reddening (Burstein and Heiles 1982).

Col. (9). Corrected V magnitude.

Col. (10). Corrected ($B-V$) color.

Col. (11). Corrected ($V-R$) color.

Figure 5 shows the color-magnitude diagram for the AGNs. The plotted ($B-V$) colors are the reddening corrected values from column (10) of Table 4. The absolute magnitudes, determined from reddening corrected visual magnitudes (col. [9] in Table 4), are plotted for two values of H_0. Objects showing a nonstellar image on the plate material used for the finding charts in Figure 2, are drawn as open circles. The line marked as B.C.E. corresponds to the mean luminosity of Sandage's (1973) brightest cluster ellipticals. The ($B-V$) color of the object 1E 1415.0+2513 has not been plotted, being very uncertain.

As can be seen from this figure the intrinsically faintest AGNs are most likely to be red in color and to be resolved. This suggests that such objects have the weakest optical nonthermal continuum emission, and the measured colors are dominated by the stellar continuum. For most of the sources brighter than the Sandage average brightest cluster ellipticals, however, the image is unresolved, and the blue colors observed are presumably dominated by nonthermal continuum emission.

In several objects shown in Figure 4 (e.g., 1E 0038.7+3251, 1E 0112.9−0147, and 1E 2124.8−1459) stellar absorption lines confirm that their reddish colors are due to a large contribution from starlight. The inverse correlation between L_x/L_{opt} and L_{opt} found for AGNs in general (Zamorani *et al.* 1981; Avni and Tananbaum 1982) favors the X-ray selection of low-luminosity AGNs such as those described above. And, of course, it is in the low-luminosity objects that the starlight contribution from the surrounding galaxy becomes relevant. But it is not clear that starlight can explain the reddish colors in all cases in Figure 5. For example, the luminous AGNs 1E 0449.4−1823 (Stocke *et al.* 1982), 1E 2204.0−4059 (spectra are shown in Fig. 7 of Paper II), 1E 0331.1−0522 (Fig. 3 herein) and 1E 1205.8+6427 (Fig. 4 herein) show no stellar absorption features and may well be similar to the luminous red quasars from the 3CR radio-selected sample (Smith and Spinrad 1980). Further optical and near-IR observations are required to determine whether starlight or an intrinsically redder continuum are responsible for the reddish colors of these and other X-ray selected AGNs.

There are four BL Lac objects present in the medium sensitivity survey sample. Our primary criteria for BL Lac classification are featureless optical continuum, detectable radio emission, and detectable optical polarization. We note that all

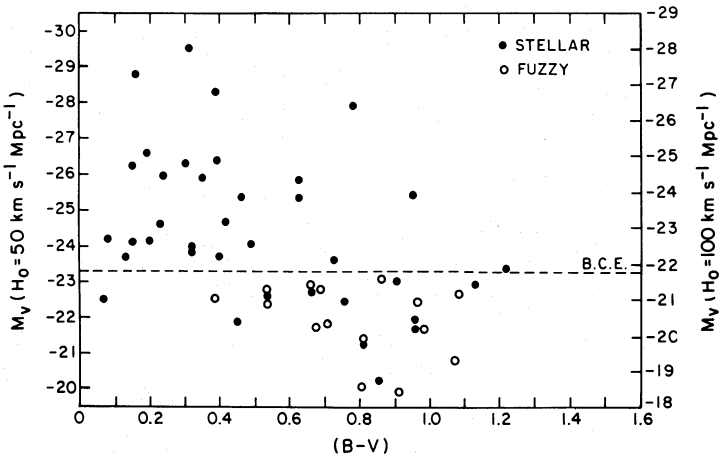

FIG. 5.—Color-magnitude diagram for the AGNs. Absolute visual magnitudes are given for two choices of Hubble constant. The luminosity corresponding to Sandage's (1973) average brightest cluster ellipticals is shown as the line marked B.C.E. Objects resolved on the plate material used for the finding charts in Fig. 2 are shown as open circles.

TABLE 4

PHOTOMETRY ON ACTIVE GALACTIC NUCLEI IN MSS 1 AND MSS 2

Source Name (1)	z (2)	V (3)	$(B-V)$ (4)	$(V-R)$ (5)	l^{II} (6)	b^{II} (7)	$E(B-V)$ (8)	V_c (9)	$(B-V)_c$ (10)	$(V-R)_c$ (11)
1E 0037.7−0157.....	0.296	17.83	0.36	0.44	116.5	−64.4	0.03	17.73	0.33	0.42
1E 0038.0+3242.....	0.197	18.25	0.45	0.97	120.3	−29.8	0.06	18.06	0.39	0.92
1E 0038.7+3251.....	0.225	18.71	1.00	1.09	120.5	−29.7	0.06	18.52	0.94	1.04
1E 0038.8−0159.....	1.690	16.92	0.34	0.42	117.1	−64.5	0.02	16.86	0.32	0.40
1E 0104.2+3153.....	2.027	18.88	0.09	0.45	126.7	−30.6	0.05	18.72	0.04	0.41
1E 0111.9−0132.....	0.120	17.73	0.98	0.55	135.9	−63.5	0.01	17.70	0.97	0.54
1E 0112.9−0147.....	0.284	18.52	1.14	0.70	136.7	−63.7	0.01	18.49	1.13	0.69
1E 0135.0+0339.....	0.637	20.45	0.92	0.37	144.4	−57.0	0.02	20.39	0.90	0.35
1E 0136.3+0605.....	0.450	18.62	0.23	0.42	143.6	−54.6	0.03	18.52	0.20	0.40
1E 0144.1−0055.....	0.080	15.95	1.08	0.10	150.3	−58.7	0.01	15.92	1.07	0.09
1E 0331.1−0522.....	0.139	17.32	0.78	0.37	190.7	−45.6	0.02	17.26	0.76	0.35
1E 0412.4−0803.....	0.037	14.94	0.99	0.85	201.0	−38.3	0.03	14.84	0.96	0.83
1E 0438.6−1049.....	0.868	19.07	0.99	0.67	207.7	−33.8	0.03	18.97	0.96	0.65
1E 0440.0−1057.....	0.279	19.53	0.48	0.96	208.0	−33.5	0.03	19.43	0.45	0.94
1E 0447.1−0917.....	0.946	18.23	0.23	0.67	207.1	−31.2	0.04	18.10	0.19	0.64
1E 0449.4−1823.....	0.338	18.38	0.76	0.54	217.3	−34.4	0.03	18.28	0.73	0.52
1E 0450.3−1817.....	0.059	17.65	0.89	0.96	217.3	−34.1	0.03	17.55	0.86	0.94
1E 0457.9−0555.....	0.303	18.10	0.18:	0.43	205.1	−27.3	0.05	17.94	0.13:	0.39
1E 0809.8+4809.....	0.459	18.16	0.46	0.49	171.4	+33.2	0.04	18.03	0.42	0.46
1E 0838.6+1324.....	0.723	18.52	0.66	0.43	213.0	+30.3	0.03	18.42	0.63	0.41
1E 0849.0+2845.....	1.273	19.19	0.42	0.56	196.5	+37.6	0.03	19.09	0.39	0.54
1E 0849.2+2829.....	0.209	19.92	1.10	0.74	196.8	+37.6	0.03	19.82	1.07	0.72
1E 0849.8+2820.....	0.197	18.93	0.99	0.77	197.0	+37.7	0.03	18.83	0.96	0.75
1E 0850.0+2828.....	1.273	19.61	0.27	0.44	196.9	+37.8	0.03	19.51	0.24	0.42
1E 0850.2+2825.....	0.922	18.37	0.33	0.51	196.9	+37.8	0.03	18.27	0.30	0.49
1E 0937.8+1153.....	0.783	18.24	0.37	0.40	222.4	+42.7	0.02	18.18	0.35	0.38
1E 1018.1+2010.....	0.250	18.54	0.54	0.43	216.5	+54.9	0.00	18.54	0.54	0.43
1E 1112.6+4059.....	0.076	17.13	0.82	0.77	172.3	+66.0	0.01	17.10	0.81	0.76
1E 1137.5+6555.....	0.397	19.58	0.72	0.14	134.2	+49.9	0.03	19.48	0.69	0.12
1E 1205.8+6427.....	0.105	17.70	0.81	0.64	130.6	+52.3	0.00	17.70	0.81	0.64
1E 1218.7+7522.....	0.645	18.26	0.49	0.30	125.6	+41.8	0.03	18.16	0.46	0.28
1E 1223.5+2522.....	0.067	16.36	0.68	0.71	231.1	+83.9	0.00	16.36	0.68	0.71
1E 1253.6−0539.....	0.420	19.97	0.54	0.79	305.1	+56.9	0.00	19.97	0.54	0.79
1E 1327.4+3208.....	0.090	16.89	0.71	0.73	64.9	+80.4	0.00	16.89	0.71	0.73
1E 1415.0+2513.....	1.057	19.67	1.21:	0.25	31.4	+70.6	0.00	19.67	1.21:	0.25
1E 1415.1+2527.....	0.560	19.49	0.40	0.31	32.1	+70.6	0.00	19.49	0.40	0.31
1E 1416.7+2524[a].....	0.674	18.86	0.23	0.08	32.2	+70.3	0.00	18.86	0.23	0.08
1E 1430.4+0527.....	0.202	17.98	0.56	0.72	355.3	+57.4	0.02	17.92	0.54	0.70
1E 1439.8−0520.....	0.620	17.43	0.21	0.38	346.5	+47.7	0.06	17.24	0.15	0.33
1E 1525.1+1550.....	0.230	16.95	0.51	0.15	23.5	+52.1	0.02	16.89	0.49	0.13
1E 1533.5+1440.....	0.021	15.55	0.83	0.78	23.2	+49.8	0.02	15.49	0.81	0.76
1E 1549.8+2022.....	0.250	17.22	0.18	0.48	33.4	+48.3	0.03	17.12	0.15	0.46
1E 1553.6+1558.....	1.324	17.71	0.79	0.51	27.8	+45.9	0.01	17.68	0.78	0.50
1E 1604.8+1552.....	0.357	19.17	0.69	0.99	29.2	+43.3	0.03	19.07	0.66	0.97
1E 1611.8−0324.....	0.298	18.10	0.48	0.67	9.0	+32.3	0.15	17.62	0.33	0.55
1E 1614.8+0533.....	0.855	18.60	0.68	0.37	18.6	+36.5	0.04	18.47	0.64	0.34
1E 1617.9+1731.....	0.116	15.29	0.10	0.27	32.9	+41.1	0.03	15.19	0.07	0.25
1E 1745.2+2747.....	0.156	17.48	0.73	0.42	52.6	+25.5	0.06	17.29	0.67	0.37
1E 2124.8−1459.....	0.057	14.81	0.90	0.82	36.8	−41.2	0.04	14.68	0.86	0.79
1E 2125.9−1456.....	0.304	18.26	1.26	1.28	36.9	−41.4	0.04	18.13	1.22	1.25
1E 2141.6+0400.....	0.410	20.11	0.10	0.61	60.3	−34.9	0.06	19.92	0.04	0.56
1E 2223.6−0517.....	1.866	17.96	0.19	0.43	58.9	−48.9	0.03	17.86	0.16	0.38
1E 2348.6+1956.....	0.043	17.22	0.95	0.94	104.2	−40.4	0.03	17.12	0.92	0.92

[a] This AGN is object labeled C in the finding chart of Paper II. Object B therein is a K star. The two objects were mislabeled in Paper II.

four BL Lac candidates have α_{ox} values considerably smaller than the mean value for X-ray selected quasars and Seyfert galaxies in the survey. All three BL Lac–defining criteria are held only by one of the candidates (1E 1402.3+0416). We are particularly concerned about the absence of optical polarization in 1E 1235.4+6315, although its Ca II H and K absorption features are extremely weak when compared to the strength of these features in normal or radio galaxies. As with the AGNs, both the more prominent stellar absorption features (compared to radio selected BL Lac objects) and the absence of optical polarization may be consequences of a large stellar fraction present in these objects.

In a future publication we will critically evaluate each BL Lac candidate, present in detail the X-ray, optical, and radio data that we have gathered on these objects, and discuss the space density of X-ray selected BL Lac objects.

VI. THE LOG $N(>S)$–LOG S RELATION

In this section we derive and discuss the log $N(>S)$–log S relation for extragalactic X-ray sources computed over the range 7×10^{-14} to 1×10^{-11} ergs cm^{-2} s^{-1} in the 0.3–3.5 keV band. The virtual complete identification rate of our sample puts us in the unique position of deriving the number-flux relation for the different classes of extragalactic objects provided enough statistics are present. This represents an advantage with respect to computing the same relation at

other wavelengths (for instance in the radio domain) where a large number of sources typically remain unidentified in any flux-limited complete sample.

The total extragalactic sample (AGNs, clusters of galaxies, BL Lac objects, and "normal" galaxies) used for the derivation of the log $N(>S)$–log S relation consists of 84 out of 112 objects. See the Notes to Table 2 for the inclusion or exclusion from the sample of those sources whose identification is ambiguous or uncertain. A nonparametric representation of the number-count relation is first obtained by determining the contribution from each source. This is done by properly weighting each source with the solid angle in which the source was visible (i.e., by considering the area of sky searched with a limiting sensitivity equal to or better than the source intensity). The integral log $N(>S)$–log S diagram is then built by summing, in decreasing flux order, the contributions from each source (see Fig. 6). We have then used the maximum-likelihood method (MLM) to determine the best fit parameters under the general assumption that the extragalactic source counts distribution can be described by a single power law. Murdoch, Crawford, and Jauncey (1973 and references therein) have shown that if the lower limit of a survey is chosen to be at least 5 times the rms noise, as it is in our case, the application of the MLM to the determination of the slope gives a minimum variance best estimate with a small correctable bias. In Paper I the application of the method and the analytical representation of the likelihood function used are given. We would like to stress that we *have not* fitted the integral distribution, the histogram shown in Figure 6. As pointed out by Jauncey as early as 1967, such a procedure is, in fact, incorrect since the numbers at each flux level are not independent. Instead, we have used the individual, ungrouped detections. Assuming for the number-flux distribution a single power law of the form $N(>S) = KS^{-\alpha}$ and maximizing the likelihood function, we obtain as the best fit to the slope the value $\alpha = 1.45$ with an associated normalization $K = 2.4 \times 10^{-15}$. The flux S is expressed in ergs $cm^{-2}\ s^{-1}$ in the 0.3–3.5 keV band over the range 7×10^{-14} to 1×10^{-11}, and N is in number of sources per steradian. The 68% (1 σ) confidence interval for α is 1.33–1.57. In Figure 6 the best fit function $N(>S) = 2.4 \times 10^{-15} S^{-1.45}$ and the $\pm 1\ \sigma$ error on the slope are plotted together with the observed distribution of the data obtained as previously described. The low flux point in the figure comes from the *Einstein* deep survey of Giacconi *et al.* (1979) and has been converted to the 0.3–3.5 keV band.

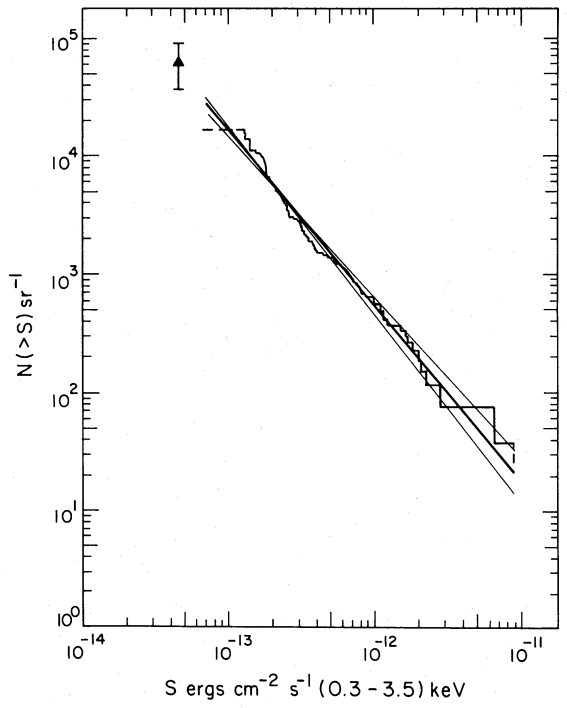

FIG. 6.—The integral log $N(>S)$–log S relation for the extragalactic X-ray sources. The low flux point is taken from the *Einstein* deep survey of Giacconi *et al.* (1979) and has been converted to the 0.3–3.5 keV band. Both the data (*histogram*) and a parametric representation are shown. Best fit (*thick line*) and $\pm 1\ \sigma$ errors on the slope (*thin lines*) are indicated. See text for details.

The value of 1.45 ± 0.12 found for the log $N(>S)$–log S slope of the extragalactic X-ray sources is in excellent agreement with the value of 1.53 ± 0.16 previously found in Paper I using MSS 1 and is consistent with the Euclidean model. As we have already pointed out in Paper I this coincidence is fortuitous, a kind of "cosmic conspiracy," and "features" are probably hidden in the log N–log S relation. In addition, MSS 1 had further suggested that the number-flux relation for extragalactic sources is, to a first approximation, the sum of two different distributions with flatter and steeper slopes, describing clusters and AGNs, respectively. With the enlarged sample now available, it is possible to separate the objects according to their nature revealing this "conspiracy". Using the same procedure adopted previously we computed the log N–log S relation for the two classes of extragalactic objects for which enough statistics are present: AGNs and clusters of galaxies. For AGNs the MLM yields, as the best value for α, 1.71 ± 0.15 with an associated normalization $K = 6.78 \times 10^{-19}$. A much flatter slope of 1.04 ± 0.23 is obtained for clusters of galaxies with an associated normalization $K = 6.88 \times 10^{-11}$. Both the observed distributions and the corresponding best fit power laws to the log N–log S relations for AGNs and clusters of galaxies are plotted in Figure 7. It is clear that, while groups and clusters of galaxies constitute the major population in extragalactic X-ray catalogs with high limiting fluxes (e.g., Forman *et al.* 1978; McHardy *et al.* 1981; Piccinotti *et al.* 1982), quasars rapidly become the dominant population when fainter fluxes are sampled. We have evidence, at more than the 90% confidence level, that indeed the "Euclidean" slope of the log N–log S is the result of two different contributions. AGNs are characterized by a fairly steep log N–log S slope as expected from the fact that they show significant cosmological evolution at X-ray wavelengths (Maccacaro *et al.* 1983; Maccacaro, Gioia, and Stocke 1984) as well as in the optical. The log N–log S of a population of objects uniformly distributed in volume has, in fact, a slope of 1.5, or even less when cosmological distance-volume effects become important (i.e., when large redshifts, $z \geq 1$, are sampled). It is worth noting also that there is no evidence of flattening at the low flux end of the AGN log N–log S. This implies the existence of a large number of X-ray sources too faint to be detected with *Einstein Observatory* and supports the conclusion of Giacconi *et al.* (1979) that a substantial fraction of the extragalactic X-ray background is due to discrete sources. Clusters of galaxies, on the other hand, have a much flatter log N–log S slope. The number of clusters of galaxies detected in the survey is still rather small, and consequently any conclusion on their evolution based on these data is, at present, premature. A further update of the Medium Sensitivity Survey is needed to obtain a larger sample of X-ray selected clusters and to allow a systematic study of their properties.

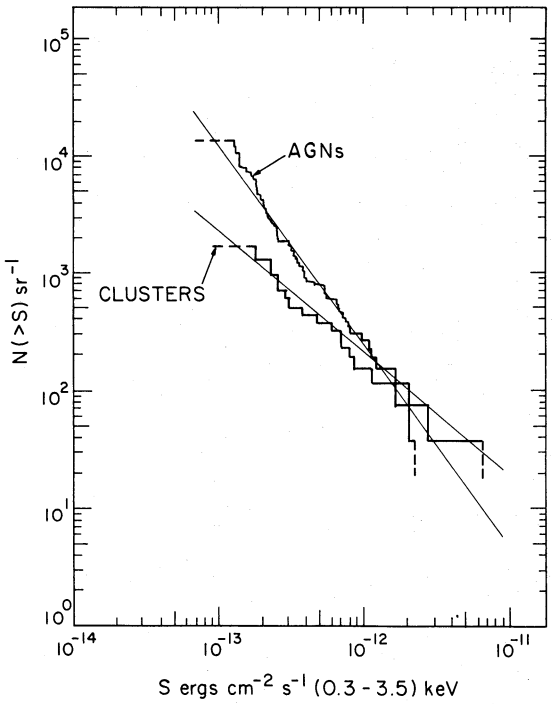

FIG. 7.—The integral log $N(>S)$–log S relations for AGNs and for clusters of galaxies. Both the best fits (*straight lines*) and the data ((*histograms*) are shown. See text for details.

VII. CONCLUSIONS

The analysis of a new set of about 150 *Einstein* IPC fields with limiting sensitivities in the range $\sim 10^{-13}$ to $\sim 10^{-12}$ ergs cm^{-2} s^{-1} (0.3–3.5 keV) has led to the discovery of 49 serendipitous sources which have been added to the already existing Medium Sensitivity Survey sample selected by Maccacaro *et al.* (1982). The combined sample consists of 112 sources detected in a total area of ~ 90 deg^2 of sky, and it is structured as a flux limited complete catalog of X-ray sources. Its size will be further expanded in the near future by analyzing additional IPC fields. A virtual 100% identification rate based on spectroscopic work has been obtained. Basically all X-ray sources in the flux range of the Medium Survey are identified with objects visible on the POSS ($m_v \leq 20.5$).

The optical content of the sample can be summarized as follows: 75% (84/112) of the sources are of extragalactic origin, while the remaining 25% are associated with galactic stars. AGNs constitute the large majority of the extragalactic population (57/84) followed by clusters and/or small groups of galaxies (18/84). BL Lacs and "normal" galaxies account for the remaining 10% of the extragalactic sample. The AGNs found in the survey are primarily low-redshift ($z \leq 1$) and low-luminosity objects, spectroscopically similar to optically or radio-selected quasars and Seyfert galaxies. However, a fraction of them ($\sim 10\%$) have quite reddish colors ($B-V \gtrsim 0.8$), similar to normal galaxies, suggesting that such objects have the weakest optical nonthermal continuum emission and that their colors are dominated by the stellar continuum.

The log $N(>S)$–log S relation has been computed for the overall extragalactic population assuming a single power law of the form $N(>S) = KS^{-\alpha}$. A value of $\alpha = 1.45 \pm 0.12$ has been found. The statistics available have allowed a meaningful computation of the source count relations for AGNs and clusters of galaxies separately. AGNs are characterized by a fairly steep log N–log S ($\alpha = 1.71 \pm 0.15$) as expected from the fact that they show a considerable amount of cosmological evolution, while the log N–log S for groups and clusters of galaxies is described by a much flatter slope ($\alpha = 1.04 \pm 0.23$).

We wish to thank the staffs of the European Southern Observatory, the Multiple Mirror Telescope Observatory, and the Steward Observatory. J. T. S. and J. W. L. thank the day crews and the night assistants at the Steward 2.3 m telescope and MMT. We particularly thank Kirk Gilmore, Bob Goff, and J. T. Williams for assistance beyond their usual duties. A particular acknowledgment goes to the Steward Observatory and the European Southern Observatory Time Allocation Committees for continuous support in granting the observation time necessary to carry on this research. We also thank John Geary who has developed and maintained CCD cameras for direct imaging at the F. L. Whipple Observatory. We thank Josh Grindlay, John Huchra, John Steiner, and Martin Ward for communicating results of optical spectroscopy on objects in several of the X-ray fields and Christine Jones for the loan of a plate for our inspection. The Kitt Peak National Observatory is thanked for the use of the POSS glass plates in preparation of the finding charts. John Black is thanked for a careful reading of the manuscript. Mark Blessing, Elizabeth Bohlen, and Mike Wenz are thanked for their careful help in the data reduction and in making finding charts. We are grateful to Linda Forbes and Joseph Singarella for assistance in the preparation of this manuscript.

This work has received partial financial support from NASA contract NAS8-30751 and from the Italian PSN (Piano Spaziale Nazionale). J. T. S. and J. W. L. acknowledge the continuing support of NASA grant NAG-8442.

APPENDIX

In Table 5 spectroscopic information is given for all objects, within the 90% confidence X-ray error circle, which were actually observed. An explanation of the columns follows.

Source Name.—X-ray source name using the same notation as in Paper I.

Obj.—Letters indicating objects as in finding charts (Fig. 2). An asterisk (*) marks those objects proposed as the optical identification of the X-ray source as in the sixth column of Table 2. A (:) sign indicates uncertain identification. A (↑) sign indicates other possible identification(s) in ambiguous cases. See Table 3 for more details.

Classific.—Optical classification for the lettered objects.

z.—Redshifts uncorrected for galactic or terrestrial motion plus error.

m_v.—Visual magnitudes measured as described in the text: one digit after the decimal point means that the magnitude was estimated from the POSS prints, while two digits indicate photometric data. A (:) sign indicates uncertain magnitude.

$\log(f_x/f_v)$.—Logarithm of X-ray to visual flux ratio computed using the formula $\log f_x/f_v = \log f_x + (m_v/2.5) + 5.37$ as described in the text (§ III).

Comments.—Comments including X-ray and spectroscopic remarks as well as radio information.

TABLE 5

SPECTROSCOPIC CLASSIFICATION OF OBJECTS IN MSS 2 X-RAY ERROR CIRCLE

Source Name	Obj.	Classific.	z	m v	log(fx/fv)	Comments
1E0013.4+1558	*A	early G star		11.8	-2.5	responsible for part of X-ray em. (see Notes to Table 2 and Table 3)
	*B	galaxy	.084±.001	16.0	1)	
	*C	galaxy	.079±.001	16.0	-0.4	
	*D	galaxy	.086±.001	14.7	1)	S(21cm) = 5.3+1.3 mJy,(Katgert et al. 1983)
	*E	mid M(e) star		16.0	-1.1	hydrogen emission, responsible for part of X-ray em. (see Notes to Table 2)
1) these values use estimated fx from a very uncertain deconvolution of each source						
1E0015.1+1603	*A	F5 star		7.4	-4.4	SAO 091825
1E0026.4+0725	*A	galaxy	.171±.001	18.27	+0.4	[OII] emission; S(6cm)=2.7mJy
	*B	galaxy	.170±.001	18.7		
	C	late F/ early G star		15.7		
1E0037.7-0157	*A	AGN	.296±.003	17.73	-0.2	type 1 (Hβ,Hγ,Hδ,Hε,[OIII], [OII])
1E0038.0+3242	*A	AGN	.197±.003	18.06	-0.1	type 1.5-2 (weak Hβ, [OIII])
	†B	early K star		13.8	-1.8	(see Table 3)
	C	early G star		14.7		
	D	mid F star		16.1		
	E	early G star		14.4		
1E0038.7+3251	*A	AGN	.225±.003	18.52	+0.3	type 1.5 (Hα broad; Hβ,[OIII], [OII] narrow; probable CaII H & K absorption)
	B	late K star		15.6	-0.8	weak Hydrogen emission
	C	G star		17.7		
	D	K star		18.0		
1E0038.8-0159	*A	AGN	1.690±.003	16.86	-0.3	type 1 (Lyα,SiIV,CIV,CIII],HeII) Strittmatter et al. 1974; S(6cm) = 322 mJy
1E0104.2+3153	*A	galaxy	.1125±.0005	16.02		
	*B	3 gal	.110 ±.005	19.2	-0.6	(see Table 3)
				18.5		
				18.8		
	*C	AGN	2.027±.001	18.72	+0.5	type 1 BAL (NV,SiIV,CIV,CIII])
	D	late G star		17.7		
	E	mid K star		18.5		
	F	G star		17.4		
1E0116.3-0116	*A	galaxy	.045±.001	15.59	-0.4	S(6cm) = 1.1 mJy
	B	early K star		15.1		
	C	galaxy	.045±.001	17.8		
1E0159.1+0330	*A	galaxy	.165±.001	18.7	+0.4	
	*B	galaxy	.160±.001	19.0		Abell 293 (see Notes to Table 2
	*C	galaxy	.165±.001	17.8	-0.1	and Table 3)
	*D	galaxy	.170±.001	17.5		
	E	late F star		14.9		
	*F	AGN	1.897±.001	20.5	+1.1	type 1 (CIV,HeII,CIII]) responsible for SE source only
	G	early M star		20.5		
	H	early F star		17.8		
1E0233.7+0649	*A	mid to late K star		13.7	-1.8	hydrogen emission
	B	early M star		19.0		
	C	late G/early K star		15.9		
1E0302.5+1716	*A	galaxy	.38±.04	20.20	+0.7	rich cluster visible on CCD frame; object A is brightest galaxy
1E0302.7+1658	*A	galaxy	.39±.04	20.13	+0.9	rich cluster visible on CCD frame; object A is brightest galaxy S(6cm) = 3.3 mJy
	B	late type star		20.2		

TABLE 5—*Continued*

Source Name	Obj.	Classific.	z	m v	log(fx/fv)	Comments
1E0303.8+1717	*A	early K star		8.7	-3.8	SAO 093280
	B	mid M star		16.0	-0.9	
	C	G star		16.2		
	D	early K star		14.3		
1E0317.0+1835	*A	BL Lac	.190±.003	18.12	+1.6	weak H & K, G band absorption optically polarized,S(6cm)=17mJy
	B	early G star		18.5		
	C	early K star		16.9		
	D	A star		16.5		
	E	mid K star		19.0		
	F	early K star		17.1		
1E0317.7-6646	:*A	early M(e) star		17.1:	-0.7	Hα emission
	B	late type star		18.5:		
	C	early K star		16.3:		
	D	G star		13.0:		
1E0326.6-2009	*A	late F star		8.9	-3.4	SAO 168572
	†B	mid G star		12.5	-1.9	north of two
	†C	early G star		12.5	-1.9	(see also Table 3 for B and C)
1E0331.1-0522	*A	AGN	.139±.001	17.26	-0.2	type 1 (Hβ,Hγ,Hδ,[OII], [OIII],[NeIII],[NeV],FeII)
1E0334.2+0025	*A	G0, RS CVn system		6.1	-2.1	SAO 111291, HR1099
1E0457.9-0555	*A	AGN	.303±.001	17.94	+0.1	type 1 (Hβ,Hγ,Hδ,[OIII])
	B	late G star		18.4		
1E0620.6-5240	*A	galaxy	.049±.001	15.1:	-0.5	PKS0620-52
	*B	galaxy	.049±.001	16.4:		
	*C	galaxy	.044±.001	17.0:		(see Notes to Table 2 and Table 3)
	*D	galaxy	.050±.001	16.4:		
	*E	galaxy	.047±.001	16.4:		
	*F	G5 star		7.5	-4.0	SAO 234461
1E0622.5-5256	A	G star		17.0:	-0.4	
	B	late F/early G star		18.2:	+0.1	
	C	late G star		19.0:	+0.4	
	D	early K star		18.7:	+0.3	
	:E	BL Lac ?		19.5:	+0.6	featureless continuumm from λλ 4300-6800 Å but spectrum noisy
	F	late G/early K star		17.0:	-0.4	
1E0623.6-5238	:A	galaxy	.076±.003	18.0::	-0.01	possible cluster
	:B	galaxy	.072±.003	18.0::		
	C	F star		13.7:	-1.7	one decade too high in fx/fv for its spectral classification
	D	G star		17.4:		
	E	late type star		18.1		
1E0730.3+6547	*A	G0 star		8.5	-3.4	SAO 014241
1E0920.5+7838	*A	G star		6.5	-4.6	SAO 006845
	†B	late F star		6.5	-4.6	(see Table 3)
1E1018.1+2010	*A	AGN	.250±.001	18.54	+0.5	type 1 (Hβ,Hγ,Hδ,[OIII], [OII], FeII)
1E1112.6+4059	*A	AGN	.076±.001	17.10	+0.5	type 1 (Hα,Hβ,Hγ,Hδ,[OIII], FeII)
	B	galaxy	.080±.003	17.7		
1E1137.5+6555	*A	AGN	.397±.001	19.48	+0.4	type 1 (MgII, Hβ)
	B	galaxy	.113±.002	18.5		strong H absorption lines
	C	early K star		17.1		
1E1205.8+6427	*A	AGN	.105±.001	17.70	+0.3	type 1 (Hβ,Hγ,Hδ,[OIII], [OII])
1E1216.1+2819	*A	mid M(e) star		15.2	-1.3	hydrogen emission
1E1218.1+7538	*A	galaxy	.0058±.0001	13.12	-1.6	NGC4291, absorption lines only

TABLE 5—*Continued*

Source Name	Obj.	Classific.	z	m v	log(fx/fv)	Comments
1E1218.7+7522	*A	AGN	.645±.001	18.16	+0.2	type 1(MgII,[OII],[NeV]) strong MgII absorp. doublet at z(emiss.) (see Fig. 3)
1E1220.0+7542	*A	galaxy	.240±.002	18.7	+0.3	[OII] emission, S(6cm)=1.9mJy
1E1235.4+6315	*A	BL Lac	.297±.002	18.52	+1.0	[OII] in emission,H & K,G band in abs., all very weak,S(6cm)=15.2mJy
1E1253.6-0539	*A	AGN	.420±.002	19.97	+0.5	type 2 ([OII],[OIII],Hβ)
1E1430.4+0527	*A	AGN	.202±.003	17.92	+0.3	type 1 (Hβ,Hγ,[OIII])
	B	early K star		17.7		
1E1439.8-0520	*A	AGN	.612±.003	17.24	-0.3	type 1 (Mg II only)
1E1522.1+3003	*A	galaxy	.116±.001	16.0:	+0.6	Abell 2069; see Gioia et al. 1982 for details
1E1553.6+1558	*A	AGN	1.324±.001	17.68	+0.3	type 1 (CIV, CIII], HeII)
1E1604.8+1552	*A	AGN	.357±.001	19.07	+0.6	type 1 (MgII,[OII],[NeIII], [NeV],Hβ,Hγ,[OIII]); FWHM(MgII) = 2000 km/s FWHM(Hβ) = 2000 km/s
	B	early K star		16.9		
	C	mid K star		16.7		
1E1611.8-0324	*A	AGN	.298±.002	17.62	-0.04	type 1 (Hβ,Hγ,Hδ,Hϵ,MgII, FeII)
	B	late K star		17.5		
	C	galaxy	.085±.001	16.5		
	D	late type star		18.9		
	E	early G star		17.5		
	F	late F star		13.4		
1E1614.8+0533	*A	AGN	.855±.003	18.47	-0.04	type 1 (MgII, [OIII]); S(6cm) = 16 mJy
1E2124.8-1459	*A	AGN	.057±.001	14.68	-1.3	type 1 (Hα,Hβ,[OIII] emission) FWHM(Hα) = 1800 km/s, abs. lines G band,Mgb,NaD present (see spectrum in Fig.4)
	B	late G star		14.4	-1.5	
	C	mid K star		17.5		
1E2125.9-1456	*A	AGN	.304±.001	18.13	+0.05	type 2 (MgII,Hβ,Hγ,[OIII],[OII]) FWHM(Hβ) < 1000 km/s
	B	mid M star		20.5		
1E2134.0+0017	:*A	mid K star		15.5	-1.1	
	B	F star		19.44	+0.5	
	C	late type star		20.0	+0.7	
1E2159.5-5714	*A	AGN	.083±.003	15.5:	-0.4	type 1
1E2316.3-4222	*A	galaxy	.054±.001	14.5:	-0.4	PKS2316-423
1E2318.2-4219	*A	AGN	.212±.002	17.0:	-0.3	type 1 (Hβ,Hγ,[OIII],FeII)
	B	F star		17.0:	-0.3	
1E2348.6+1956	*A	AGN	.043±.001	17.12	-0.04	type 2 (Hα,Hβ,[OIII],[NII]) S(6cm) = 2.2 mJy
1E2349.9+1951	*A	early K star		11.0	-2.7	
	B	late G/early K star		14.5	-1.3	
	†C	galaxy	.084±.003	16.98	-0.3	(see Table 3)
	D	early G star		16.9		
	E	galaxy	.103±.003	18.7		

REFERENCES

Avni, Y., and Tananbaum, H. 1982, *Ap. J.* (*Letters*), **262**, L17.
Burstein, D., and Heiles, C. 1982, *A.J.*, **87**, 1165.
Chanan, G. A., Margon, B., and Downes, R. A. 1981, *Ap. J.* (*Letters*), **243**, L5.
Elvis, M., Schreier, E., Tonry, J., Davis, M., and Huchra, J. 1981, *Ap. J.*, **246**, 20.
Feigelson, E. D., Maccacaro, T., and Zamorani, G. 1982, *Ap. J.*, **255**, 392.
Forman, W., Jones, C., Cominsky, L., Julien, P., Murray, S., Peters, G., Tananbaum, H., and Giacconi, R. 1978, *Ap. J. Supplement*, **38**, 357.
Fraquelli, D. A. 1982, *Ap. J.* (*Letters*), **254**, L41.
Giacconi, R., *et al.* 1979, *Ap. J.* (*Letters*), **234**, L1.
Gioia, I. M., Geller, M. J., Huchra, J. P., Maccacaro, T., Steiner, J. E., and Stocke, J. 1982, *Ap. J.* (*Letters*), **255**, L17.
Gioia, I. M., Feigelson, E. D., Maccacaro, T., Schild, R., and Zamorani, G. 1983, *Ap. J.*, **271**, 524.
Gioia, I. M., and Maccacaro, T. 1983, in *Proceedings of the 24th Liège Astrophysical Colloquium Quasars and Gravitational Lenses* (Liège: Institut d'Astrophysique), p. 63.
Griffiths, R. E., *et al.* 1983, *Ap. J.*, **249**, 375.
Jauncey, D. L. 1967, *Nature*, **216**, 877.
Johnson, H. L. 1966, *Ann. Rev. Astr. Ap.*, **4**, 193.
Katgert, P., Thuan, T. X., and Windhorst, R. A. 1983, *Ap. J.*, **275**, 1.
King, I., and Raff, M. 1977, *Pub. A.S.P.*, **89**, 120.
Kriss, G. A., and Canizares, C. R. 1982, *Ap. J.*, **261**, 51.
Maccacaro, T., *et al.* 1982, *Ap. J.*, **253**, 504 (Paper I).
Maccacaro, T., Avni, Y., Gioia, I. M., Giommi, P., Griffiths, R. E., Liebert, J., Stocke, J., and Danziger, J. 1983, *Ap. J.* (*Letters*), **266**, L73.
Maccacaro, T., and Gioia, I. M. 1983, in *IAU Symposium 104, Early Evolution of the Universe and its Present Structure*, ed. G. O. Abell and G. Chincarini (Dordrecht: Reidel), p. 7.
Maccacaro, T., Gioia, I. M., and Stocke, J. T. 1984, *Ap. J.*, **283**, 486.
Margon, B., Chanan, G. A., and Downes, R. A. 1982, *Ap. J.* (*Letters*), **253**, L7.
McHardy, I. M., Lawrence, A., Pye, J. P., and Pounds, K. A. 1981, *M.N.R.A.S.*, **197**, 893.
Murdoch, H. S., Crawford, D. F., and Jauncey, D. L. 1973, *Ap. J.*, **183**, 1.
Piccinotti, G., Mushotzky, R. F., Boldt, E. A., Holt, S. S., Marshall, F. E., Serlemitsos, P. J., and Shafer, R. A. 1982, *Ap. J.*, **253**, 485.
Reichert, G. A., Mason, K. O., Thorstensen, J. R., and Bowyer, S. 1982, *Ap. J.*, **240**, 437.
Sandage, A. 1973, *Ap. J.*, **183**, 731.
Schild, R. E. 1984, in preparation.
Smith, H. E., and Spinrad, H. 1980, *Ap. J.*, **236**, 419.
Smithsonian Astrophysical Observatory Star Catalog (Washington: Smithsonian Institution, 1966).
Stocke, J., Liebert, J., Gioia, I. M., Griffiths, R. E., Maccacaro, T., Danziger, I. J., Kunth, D., and Lub, J. 1983, *Ap. J.*, **273**, 458 (Paper II).
Stocke, J., Liebert, J., Maccacaro, T., Griffiths, R. E., and Steiner, J. E. 1982, *Ap. J.*, **252**, 69.
Stocke, J. T., Liebert, J. W., Schild, R., Gioia, I. M., and Maccacaro, T., 1984, *Ap. J.*, **277**, 43.
Strittmatter, P. A., Carswell, R. F., Gilbert, G., and Burbidge, E. M. 1974, *Ap. J.*, **190**, 509.
Tucker, W. H. 1983, *Ap. J.*, **271**, 531.
Wolfe, A., ed. 1978, *Pittsburgh Conference on BL Lac Objects* (Pittsburgh: University of Pittsburgh).
Zamorani, G., *et al.* 1981, *Ap. J.*, **245**, 357.

I. J. DANZIGER: European Southern Observatory, 8046 Garching bei München, Federal Republic of Germany.

I. M. GIOIA, T. MACCACARO, and R. E. SCHILD: Harvard-Smithsonian Center for Astrophysics, 60 Garden Street, Cambridge, MA 02138

D. KUNTH: Institut d'Astrophysique, 98 bis Bd. Arago, F-75014 Paris, France

J. W. LIEBERT and J. T. STOCKE: Steward Observatory, University of Arizona, Tucson, AZ 85721

J. LUB: Sterrewacht, Leiden, 2300 RA Leiden, The Netherlands

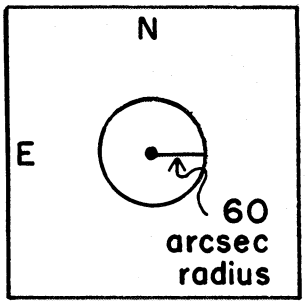

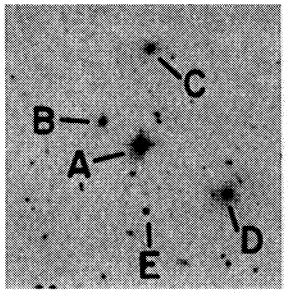

0013.4+1558

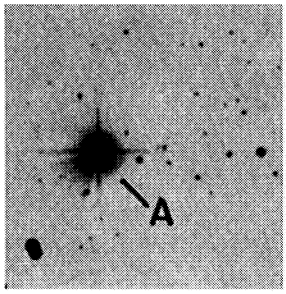

0015.1+1603

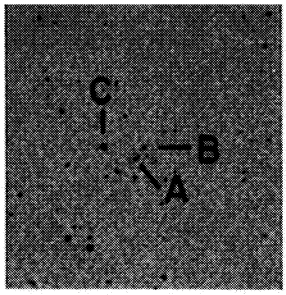

0026.4+0725

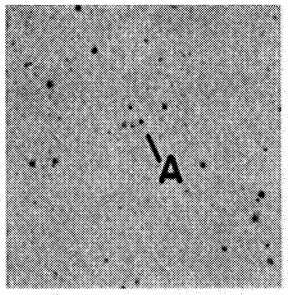

0037.7−0157

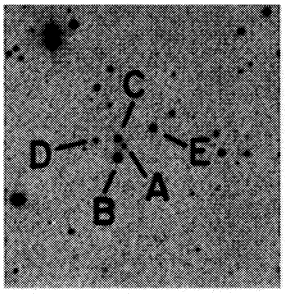

0038.0+3242

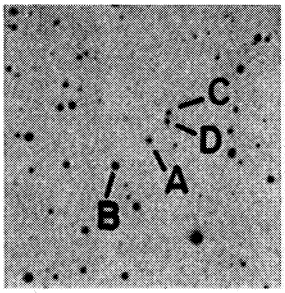

0038.7+3251

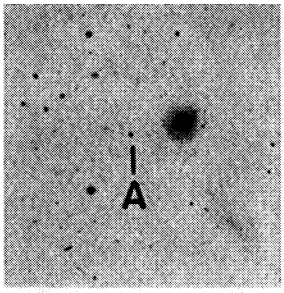

0038.8−0159

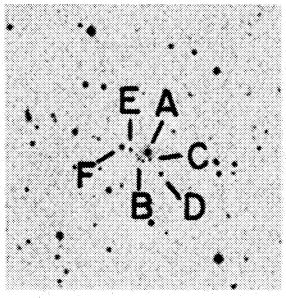

0104.2+3153
O PLATE

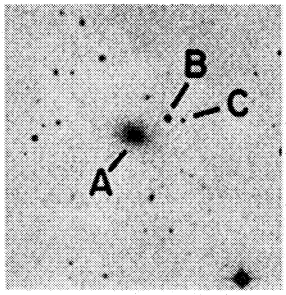

0116.3−0116

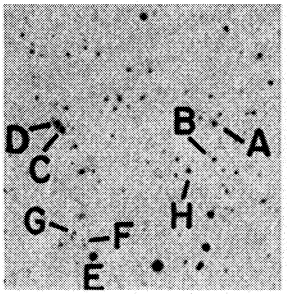

0159.1+0330

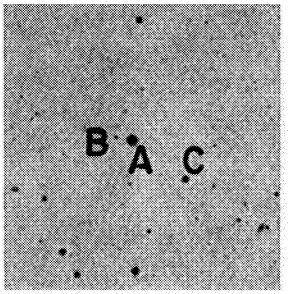

0233.7+0649

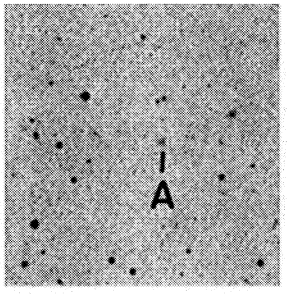

0302.5+1716

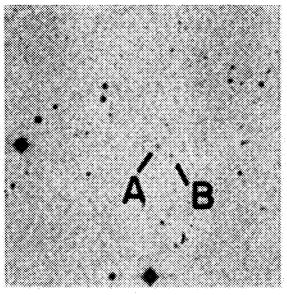

0302.7+1658

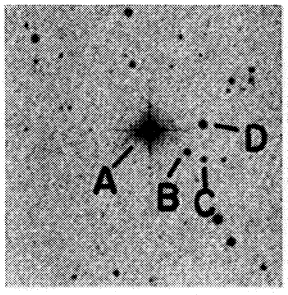

0303.8+1717

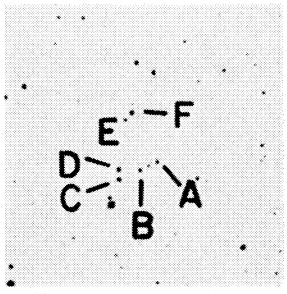

0317.0+1835

FIG. 2.—Finding charts for the Medium Survey sources listed in Table 2. All but the last chart are reproductions from the Palomar Observatory Sky Survey red plates unless otherwise noted. Each chart is centered on the X-ray source centroid. The marked objects were spectroscopically observed and are described either in Table 2 or in the Appendix. The last plate contains finding charts for three fields which are obscured by Canopus on the ESO or SRC Schmidt plates. This plate is a reproduction of a red (IIIa-F + RG630) SRC Schmidt plate. "Plate flaws" are circled, and the X-ray centroid for each source is marked with an X. The NE quadrant of Canopus has been "dodged" on this reproduction to more clearly show the optical objects near 1E 0623.6−5238.

GIOIA (*see* page 500)

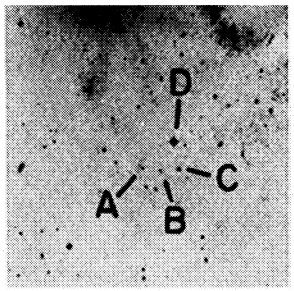

0317.7−6646
SRC J PLATE

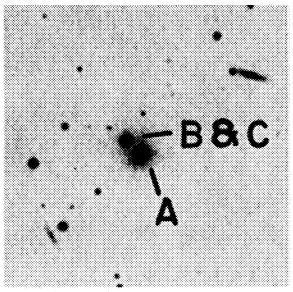

0326.6−2009

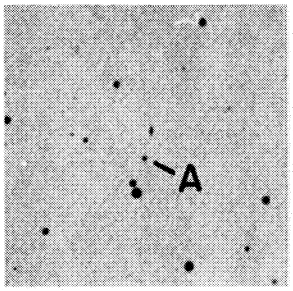

0331.1−0522

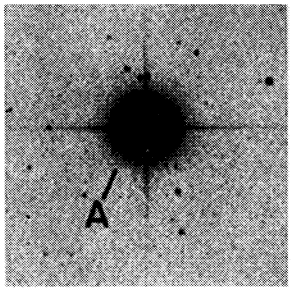

0334.2+0025

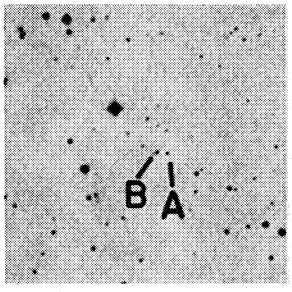

0457.9−0555

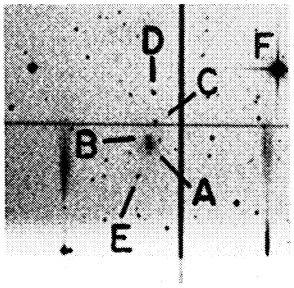

0620.6−5240
ESO BLUE

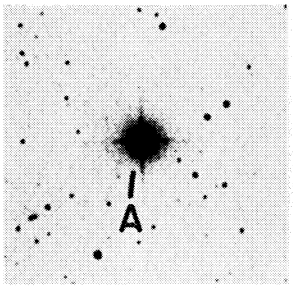

0730.3+6547

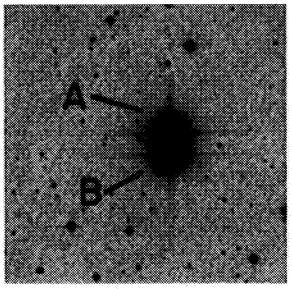

0920.5+7838

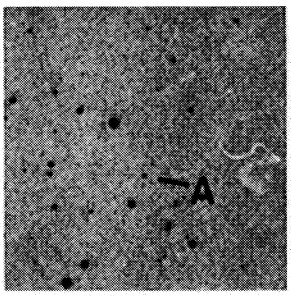

1018.1+2010

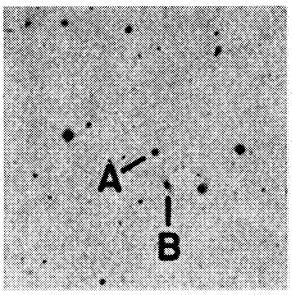

1112.6+4059

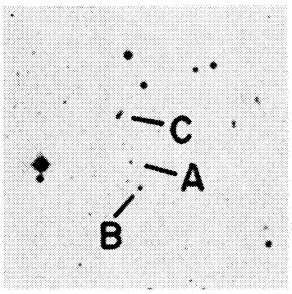

1137.5+6555
O PLATE

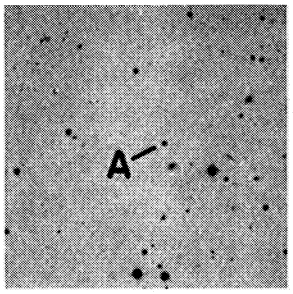

1205.8+6427

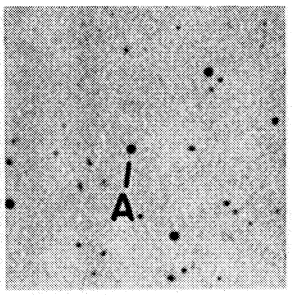

1216.1+2819

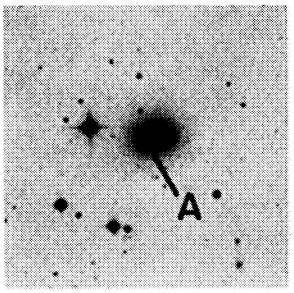

1218.1+7538

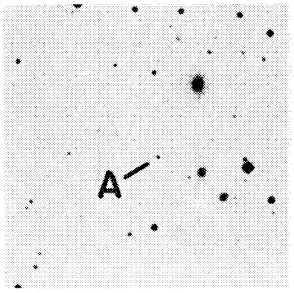

1218.7+7522

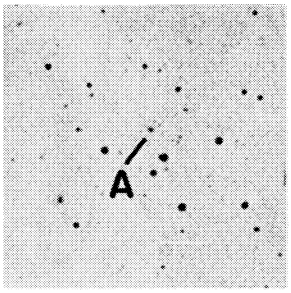

1220.0+7542

FIG. 2.—*Continued*

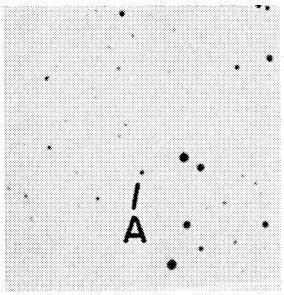

1235.4 + 6315

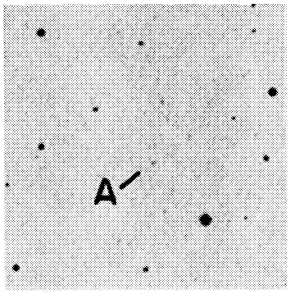

1253.6 − 0539
O PLATE

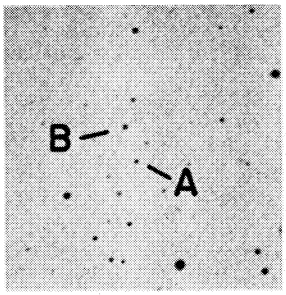

1430.4 + 0527

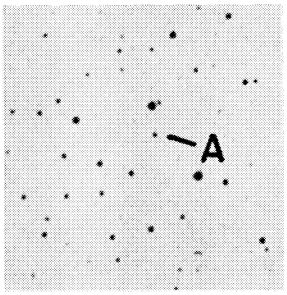

1439.8 − 0520

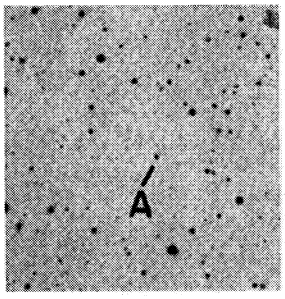

1553.6 + 1558

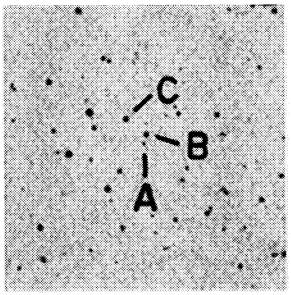

1604.8 + 1552

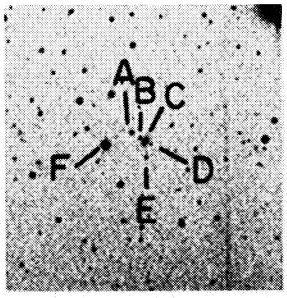

1611.8 − 0324

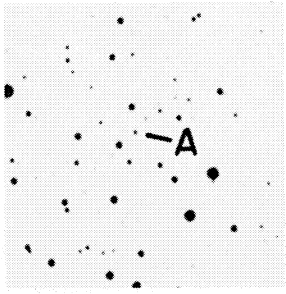

1614.8 + 0533
O PLATE

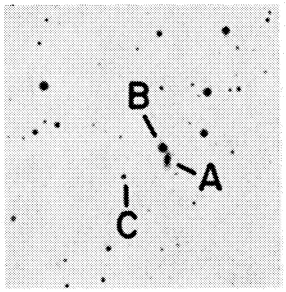

2124.8 − 1459

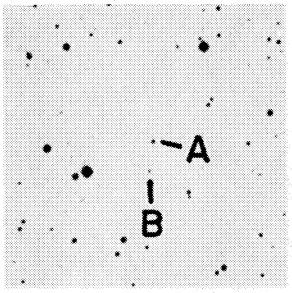

2125.9 − 1456

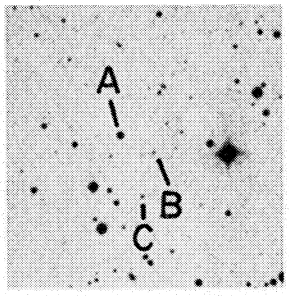

2134.0 + 0017
O PLATE

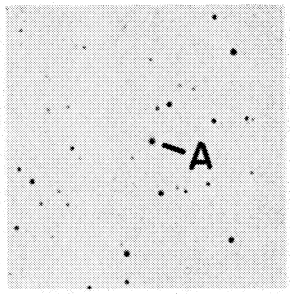

2159.5 − 5714
ESO BLUE

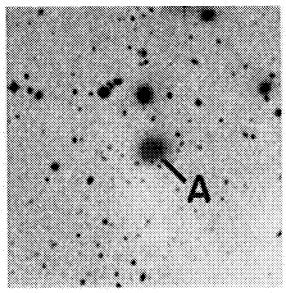

2316.3 − 4222
SRC J PLATE

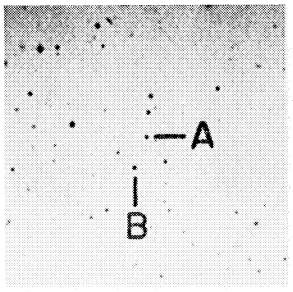

2318.2 − 4219
SRC J PLATE

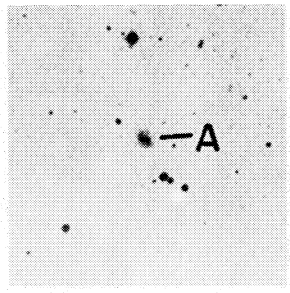

2348.6 + 1956

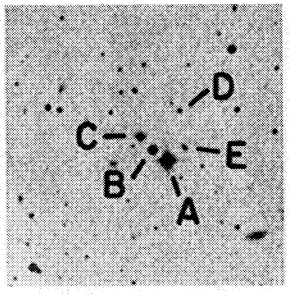

2349.9 + 1951

FIG. 2.—*Continued*

GIOIA (*see* page 500)

PLATE 13

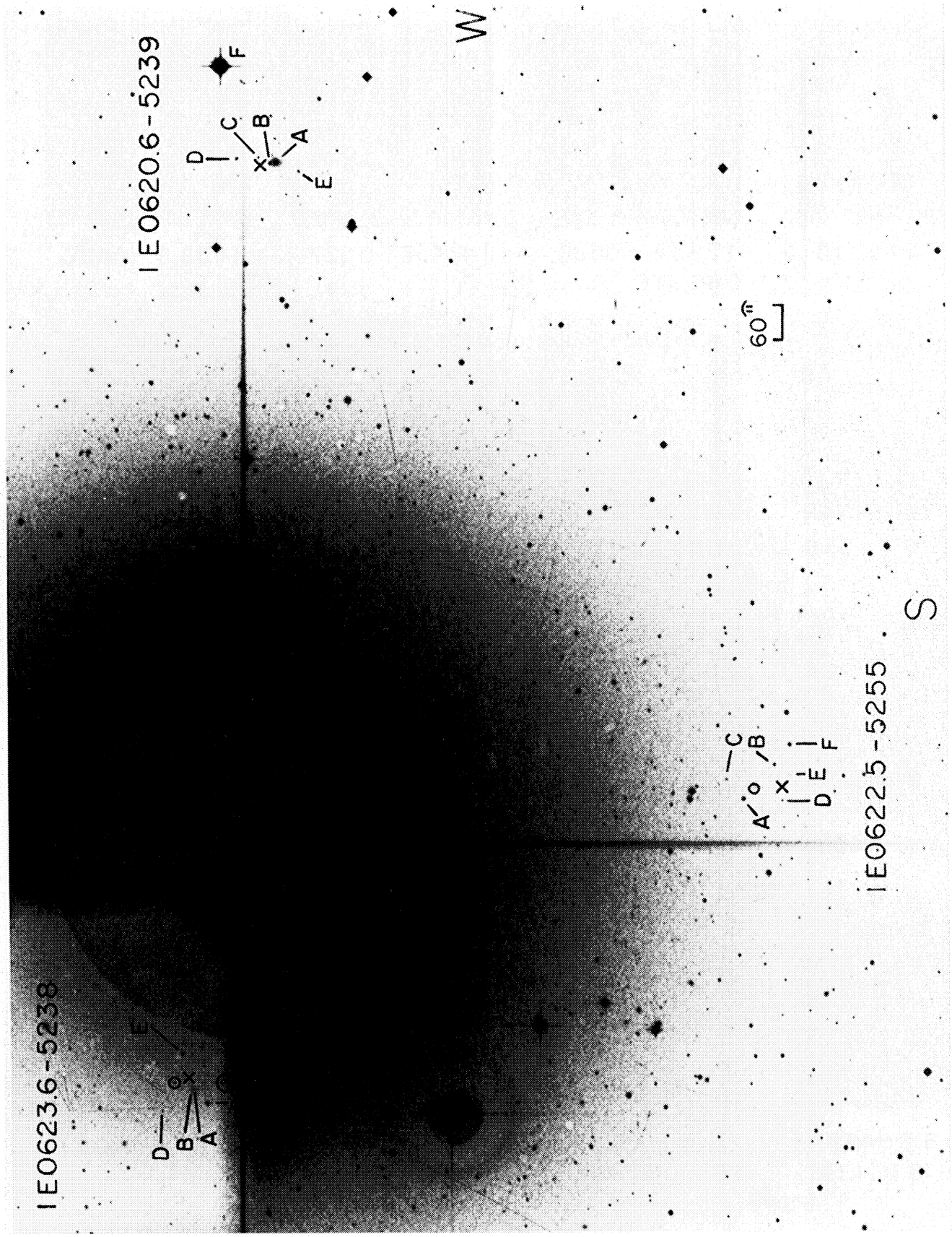

FIG. 2.—*Continued*